Master's Thesis in Engineering

# Anti-obesity Effect of *Trans*-anethole and *Trans*-cinnamic Acid by Induction of Fat Browning

Department of Biotechnology

Nam Hyeon Kang

Supervising Professor Jong Won Yun

August, 2019

Graduate School of Daegu University

# Anti-obesity Effect of *Trans*-anethole and *Trans*-cinnamic Acid by Induction of Fat Browning

In Partial Fulfillment of the Requirements for the Degree of Master of Engineering.

Department of Biotechnology

Nam Hyeon Kang

Supervising Professor Jong Won Yun

Confirming Nam Hyeon Kang's Master's Thesis in Engineering.

August, 2019

Chairman of Committee _____ (Signature)

Member of Committee _____ (Signature)

Member of Committee _____ (Signature)

Graduate School of Daegu University

# CONTENTS

# LIST OF TABLES

# LIST OF FIGURES

# Anti-obesity Effect of *Trans*-anethole and *Trans*-cinnamic Acid by Induction of Fat Browning

Nam Hyeon Kang

Department of Biotechnology
Graduate School, Daegu University
Gyeongbuk, Korea

Supervised by Prof. Jong Won Yun

(Abstract)

Browning of white adipocytes and activation of brown adipocytes suggests attractive strategy for prevention of obesity. The use of natural compounds for browning is regarded as a safe and new strategy for anti-obesity. Here, we report that *trans*-anethole (TA), a flavoring substance present in the essential oils of various plants and *trans*-cinnamic acid (*t*CA), a class of cinnamon from the bark of Cinnamomum cassia, induced browning in white adipocytes. TA and *t*CA increased protein content of brown-fat specific markers (PGC-1α, PRDM16, and UCP1) and expression levels of beige-fat-specific genes (Cd137, Cited1, Tbx1, and Tmen26) in 3T3-L1 white adipocytes, as well as brown-fat-specific genes (Cidea, Lhx8, Ppargc1, Prdm16, Ucp1, and Zic1) in HIB1B brown adipocytes. In addition, TA and *t*CA increased fat oxidation, reduced adipogenesis and lipogenesis in 3T3-L1 adipocytes, and activated HIB1B adipocytes. Further, mechanistic study revealed that TA and *t*CA induced browning of 3T3-L1 adipocytes by activating the β3-AR and AMPK signaling pathways. Specially, TA induced browning via regulation of not only β3-AR but also the AMPK-mediated SIRT1 pathway. Moreover, in vivo study on TA revealed its efficiency as a potent anti-obesity agent by alleviating thermogenesis, suggesting its potential to treat obesity and its related metabolic disorders.

# CHAPTER 1

*Trans*-anethole ameliorates obesity via induction of browning in white adipocytes and activation of brown adipocytes

# 1. Introduciton

Obesity is a serious health problem that has become one of the mos t common health concerns of modern times. Adipose tissue has increasingl y become an area of focus for researchers since it plays an important role in the human body not only in fat accumulation but also in endocrine roles (Virtanen et al., 2009; Bonet et al., 2014). To treat obesity, suppression of white adipose tissue (WAT) expansion and activation of brown adipose tis sue (BAT) are considered as potential therapeutic targets (Lee et al., 2014) In particular, recent advancements have been made in utilizing BAT functi on, which increases oxidative metabolism at the expense of fat storage in order to dissipate energy as heat (Calderon-Dominguez et al., 2016). Rece ntly, induction of the brown fat-like phenotype in WAT (formation of *brite* or beige adipocytes) represents another attractive potential strategy for the management and treatment of obesity (Calderon-Dominguez et al., 2016; va n Marken Lichtenbelt et al., 2009; Harms et al., 2013). Apart from classical BAT, recruitment of beige adipocytes has been observed in WAT depots i n response to specific stimuli such as chronic cold exposure, endogenous signals, as well as dietary factors and pharmacological agents (Bonet et al., 2014; Azhar et al., 2016).

Due to the serious side effects of synthetic anti-obesity medicines i n the commercial market, many natural products with anti-obesity effects have recently become more appealing to consumers (Vermaak et al., 2011). Of note, a wide variety of natural compounds are known to favor the acq uisition of brown adipocyte-like features in white adipocytes (Bonet et al., 2014; Lone et al., 2015; Azhar et al., 2016; Lone et al., 2016; Parray et al., 2015; Choi et al., 2016; Choi., 2016). In the screening of natural anti-obesity compounds, we observed that *trans*-anethole possessed the capacity to recr

uit beige adipocytes both in cultured 3T3-L1 adipocytes and obese mice fed a high fat diet.

*Trans*-anethole (*trans*-1-methyoxy-4-propenyl-benzene, Fig. 1A) is a flavoring substance present in the essential oils of various plants of more than 20 species, including fennel, anise, and star anise, and has been used for culinary purposes for centuries (Bartonkova et al., 2017). Two isomers of anethole occur in nature: E- or *trans*-anethole and Z- or cis- anethole. About 90% of natural anethole is *trans*-anethole (TA), and only TA is considered as food grade due to the higher toxicity of cis-anethole (Aprotosoaie et al., 2016). Although TA was accorded Generally Recognized as Safe status by the FDA, several toxicity studies have reported carcinogenicity in high dose animal groups (Stoner et al., 1973; Miller et al., 1983). A long-term feeding study reported that TA is unlikely to be a rodent carcinogen and can thus be considered as non-genotoxic and non-carcinogenic (Truhaut et al., 1989; Gorelick., 1995). TA has been widely used as a flavor agent in foods, cosmetics, and perfumes and attempts to explore its pharmaceutical potential in human chronic diseases have recently been made (Aprotosoaie et al., 2016). Animal and cell line data suggest that TA may have beneficial effects in several chronic diseases, including cancer (Chen et al., 2009; Chen et al., 2012), diabetes (Dongare et al., 2012; Sheikh et al., 2015), inflammation (Freire et al., 2005; Kang et al., 2013), wound-healing (Cavalcanti et al., 2012), immunomodulation (Wizzler et al., 2015), as well as neurological (Ryu et al., 2014) and skin diseases (Galicka et al., 2014), where several molecular targets of TA have been partly identified (Aprotosoaie et al., 2016).

Recent advances in the field of bioinformatics have provided detailed perspectives and an intense understanding of interacting proteins at the molecular level, highlighting modulation of protein behavior due to binding

of small drug-like compounds forming complexes (Sadiq et al., 2013). Molecular docking data contributes to determination of the mechanisms of action driving protein interactions by imparting insights into structural stability, energy levels of binding modes, and selectivity of unique residues of amino acids, which play major roles during intermolecular interactions (Bhattacharjee et al., 2015). Thus, *in silico* analytical tools were considered and utilized to characterize the molecular relationships between lipid metabolic proteins and our compound of interest.

To date, the anti-obesity effect of TA has not been reported. The objective of the present study was to investigate the anti-obesity effect of TA by stimulating thermogenic activity through induction of the *beige* phenotype in cultured 3T3-L1 white adipocytes as well as on diet-induced obese mice and activation of brown adipocytes. Further validation by computational techniques was performed to improve our understanding about the mechanism of action of TA on browning pathways.

## 2. Materials and methods

### 2.1 Chemicals

*Trans*-anethole (99% purity) and resveratrol were purchased from Sigma Chemical Co. (St. Louis, MO, USA). BRL 37344 and L-748.337 were purchased from Tocris Bioscience (Bristol, UK). EX527 was purchased fro m Selleckchem (Houston, TX, USA). All other chemicals used in this stud y were of analytical grade.

### 2.2 Cell culture and differentiation

Dulbecco's Modified Eagle's Medium (DMEM, Thermo, Waltam, M A, USA) supplemented with 10% fetal bovine serum (FBS, Thermo), and 1 00 μg/ml of penicillin-streptomycin (Thermo) was used to culture 3T3-L1 (ATCC, Manassas, VA, USA) at 37ºC in a 5% $CO_2$ incubator. Sufficiently confluent cells were maintained in differentiation induction medium consisti ng of 10μg/ml of insulin (Sigma, St. Louis, MO, USA), 0.25 μM dexametha sone (Dex, Sigma), and 0.5mM 3-isobutyl-1-methylxanthine (IBMX, Sigm a) in DMEM, followed by maturation medium containing 10% FBS and 1 0μg/ml of insulin. During treatments, unless otherwise stated, cells were m aintained in complete medium containing 100 μM TA (dissolved in 99% eth anol )for 6-10 days before further analysis, and maturation mediumwas cha nged every 2 days. Cytotoxicity of TA was evaluated by MTT assay as d escribed previously (Mosmann., 1983).

### 2.3 Animal experiments

Five-week-old C57BL/6 mice were acclimatized with normal chow for 1 week and then divided into two groups *viz*. HFD (60% fat)-fed contr

ol mice (CON group) and HFD-fed mice treated with TA by oral administ ration (TA group). TA was administered daily by oral gavage to mice at a dose of 100 mg/kg body weight for 8 weeks. In order to minimize volatil ization during TA feeding, stock solution of TA was prepared as a small a liquot dissolved in 30% ethanol. All animal experiments were approved by the Committee for Laboratory Animal Care and Use of Daegu University.

### 2.4 Quantitative real-time RT-PCR

Total RNA was isolated from mature cells (4-10 days) using a tota l RNA isolation kit (RNA-spin, iNtRON Biotechnology, Seongnam, Korea). RNA (1 μg) was converted to cDNA using Maxime RT premix (iNtRON Biotechnology). Power SYBR green (Roche Diagnostics Gmbh, Mannheim, Germany) was employed to quantitatively determine transcription levels of genes with RT-PCR (Stratagene 246 mix 3000p QPCR System, Agilent Te chnologies, Santa Clara, CA, USA). PCR reactions were run in duplicate fo r each sample, and transcription levels of all genes were normalized to the level of *β-actin*. Sequences of primer sets used in this study are listed in Table 1.

### 2.5 Oil Red O staining

Cells were matured for 4-8 days, followed by washing with phosph ate-buffered saline (PBS), fixation with 10% formalin for 1 h at room temp erature, and washing again three times with deionized water. A mixture of Oil Red O solution (0.6% Oil Red O dye in isopropanol) and water at a 6: 4 ratio was layered onto cells for 20 min, followed by washing four times with deionized water, and images were captured under a microscope.

## 2.6 Immunoblot analysis

Cell lysates were prepared using RIPA buffer (Sigma) by homogeni zation and centrifugation at 14000 ×*g* for 20 min. Cell extract was diluted in 5X sample buffer (50 mM Tris at pH 6.8, 2% SDS, 10% glycerol, 5% β-mercaptoethanol, and 0.1% bromophenol blue) and heated for 5 min at 9 5°C before 8, 10, or 12% SDS-polyacrylamide gel electrophoresis (PAGE). After electrophoresis, samples were transferred onto a polyvinylidene difluo ride membrane (PVDF, Santa Cruz Biotechnology, Santa Cruz, CA, USA) a nd then blocked for 1 h with TBS-T (10 mM Tris-HCl, 150 mM NaCl, an d 0.1% Tween 20) containing 5% skim milk or BSA (Rocky Mountain Biol ogicals, Missoula, MT, USA). The membrane was rinsed three times conse cutively with TBS-T buffer, followed by incubation for 1 h with 1:1,000 di lutions of primary polyclonal antibodies, including anti-ATGL, anti-β-actin, anti-PPARα, anti-PPARɣ, anti-AMPK, anti-pAMPK, anti-PRDM16, anti-U CP1, anti-PGC-1α, anti-CPT1, anti-ACOX1, anti-C/EBPα, anti-β3-AR, anti -PKA, anti-SIRT1, anti-FAS (Santa Cruz Biotechnology), anti-ACC, anti-p ACC (Cell Signaling Technology, Beverly, MA, USA), and anti-pHSL (Ab cam, Cambridge, UK), in TBS-T buffer containing 1% skim milk or BSA. After three washes, the membrane was incubated for 1 h with horseradish peroxidase-conjugated anti-goat IgG, anti-rabbit IgG, or anti-mouse IgG se condary antibody (1:1000, Santa Cruz Biotechnology) in TBS-T buffer cont aining 1% skim milk or BSA. Development was carried out using enhanced chemiluminescence (West Zol, iNtRON Biotechnology). Quantification of ban d intensities was performed by using ImageJ software (NIH).

## 2.7 Hematoxylin and eosin staining

For the histological study, inguinal WAT (iWAT), epididymal WAT (eWAT), and BAT were separately fixed in 10% neutral-buffered formalin,

washed with PBS, and embedded in paraffin wax. Paraffin-embedded tissue sections (3-5 $\mu$m each) were deparaffinized, rehydrated, and subjected to hematoxylin (Vector Laboratories Inc, CA, USA) and eosin (Daejung, Siheung, Republic of Korea) (H&E) staining. Histopathological findings were observed using light microscopy (X20 Olympus IX51, Tokyo, Japan).

### 2.8 Immunofluorescence

Immunohistochemistry was then performed on formalin-fixed, paraffin-embedded tissues. The sections were then incubated with primary antibody, anti-UCP1 (dilution 1:1000, Santa Cruz Biotechnology), overnight at 4 C, followed by incubation with appropriate rhodamine goat anti-rabbit secondary antibody at room temperature for 4 h. For staining of mitochondria, MitoTracker®green (1mM, Cell Signaling Technology) was directly added to PBB-T at a concentration of 200 nM, and tissues were kept for 2 h at 37°C. After incubation, tissues were washed with PBS and subjected to immunostaining. The histopathological findings were observed using light microscopy at X20 magnification.

### 2.9 Infrared thermography

To determine the surface body temperature of mice, all animals were kept in small boxes with bodies positioned in a straight position and the upper back area to neck region exposed. A thermal imaging camera (Therm-App TA19A17Q-1000, thermal imaging device with 19 mm lens) was used to acquire skin temperature images. All images were taken at room temperature.

### 2.10 Transmission electron microscopy (TEM)

Inguinal WAT of mice were washed with 0.1 M phosphate buffer and fixed in 2.5% (w/v) glutaraldehyde solution overnight at 4°C. After three washes in 0.1 M phosphate buffer, tissues were post-fixed with 1% (w/v) osmium tetroxide in 0.1 M phosphate-buffer for 1 h. Tissue samples were dehydrated with an increasing concentration of ethanol and embedded with epoxy resin. Ultra-thin sections (70-80 nm) were cut and stained with uranyl citrate and lead citrate before being examined under a transmi ssion electron microscope H-7600 with X2.5k magnification (Hitachi, Tokyo, Japan).

### 2.11 In silico analysis

A molecular docking study was carried out to analyze the interactio ns of TA with target proteins that promote browning and regulate lipid metabolism. The investigation included different modules of Schrödinger sof tware (Schrödinger, LLC, New York, NY, 2017).

#### 2.11.1 Retrieval and processing of target protein structures

The target proteins selected for docking studies were screened on t he basis of their involvement in the WAT browning mechanism (Suppleme ntary Table 1). The 3-D structures for the list of target proteins (Supplem entary Fig. 1) were retrieved from the RCBS PDB database (https://www.r csb.org/). Some protein structures indicate the presence of predefined ligan ds, which were optimized prior to initiation of docking using the Protein Pr eparation Wizard (Schrödinger Release 2017-4: Schrödinger Suite 2017-4 Pr otein Preparation Wizard; Epik, 2016; Impact, 2016; Prime, 2017). The crite

ria for processing of protein files were implemented to eliminate inconsisten cies in structure comprising addition of missing chains, loops, inclusion of missing hydrogens, correction of bond order, adjustment of ionization prope rties, and refinement of geometry with rectified orientation of the various f unctional groups of amino acids. The minimized structures for target prote ins were then used for ligand docking.

### 2.11.2 Binding site prediction

The possible active sites utilized for binding to ligand-based compo unds were predicted for every target protein using the Schrödinger applicat ion SiteMap (Schrödinger Release 2017-4: SiteMap., 2017).

### 2.11.3 Retrieval and preparation of ligand structure

The 3-D crystal structure of TA (Supplementary Fig. 2) was retrie ved from the NCBI Pubchem database (https://pubchem.ncbi.nlm. nih.gov/). The structure was then minimized by Schrödinger Application Ligprep (Schrödinger Release 2017-4: LigPrep, Schrödinger., 2017) based on the cha rges added and detection of rotatable bonds. Two possible poses for the ligand were generated after minimization of the ligand, and the best pose was selected for docking with the target proteins.

### 2.11.4 Molecular docking

Two types of docking were performed for the validation of binding energies. Individual docking was carried out by Schrödinger Application Gli de Ligand Docking (Schrödinger Release 2017-4: Glide., 2017). For detection of protein conformation changes, Schrödinger Application Induced Fit Dock ing was also performed (Schrödinger Release 2017-4: Schrödinger Suite 201

7-4 Induced Fit Docking protocol; Glide., 2016; Prime., 2017). Binding affinities were also determined to predict the best target protein using Schrödinger application Prime-MMGBSA (Schrödinger Release 2017-4: Prime., 2017). Glide was comprised of Grid-based Ligand docking, for which the grid was generated based on the binding sites predicted by SiteMap for each target protein used for comparison of the binding sites for the ligand. Flexible docking was performed in Extra-Precision (XP) mode in Glide. Schröding er provides a Glide-score for determination of pose and binding energies in Kcal/mol, and Glide-score (G-score) was calculated by the software as G-Score = 0.065*vdW + 0.130*Coul + Lipo + HBond + Metal + BuryP + RotB + Site (vdW, van der Waals energy; Coul, Coulomb; Lipo, lipophilic term; HBond, hydrogen bonding; Metal is metal-ion binding term; BuryP, buried polar groups' penalty; RotB, penalty for rotatable bonds that has been frozen; Site, active site polar interaction) (Subhani et al., 2015). The following formula was used to convert the binding energies into International Standard Unit: $E_{(KJ)} = 4.184 * E_{(Kcal-IT).}$

### 2.11.5 Estimation of ligand-binding affinity

The binding affinity of each target protein for TA was evaluated using the Prime-MMGBSA module of Schrödinger (Schrödinger Release 2017-4: Prime, 2017). Prime-MMGBSA dG Bind is the binding free energy, which was calculated with the equation: - ΔG (bind)= E_complex (minimized)- E_ligand (minimized)+E_receptor (minimized), where E_complex is the minimized total energy of the complex, E_ligand is the minimized energy of the ligand, and E_receptor is the minimized energy for the receptor. All these energy terms are a combination of Coulomb energy, covalent binding energy, van der Waals energy, lipophilic energy, hydrogen-bonding energy, polar interaction, and self-contact correction.

## 2.12 Statistical analysis

All data were expressed as the mean ± SD, and comparison was made by using the Statistical Package of Social Science (SPSS, version 17.0; SPSS Inc., Chicago, IL, USA) program, followed by Tukey's post-hoc tests or Student's *t*-test. Statistical significances between control and TA-treated groups were indicated as either $p<0.05$ or $p<0.01$.

# 3. Results

## 3.1 *Trans*-anethole (TA) induces browning of 3T3-L1 white adipocytes

Firstly, TA cytotoxicity in 3T3-L1 preadipocytes was evaluated by MTT assay. As shown in Fig. 1B, no significant cytotoxicity was observe d up to 100 μM TA. Hence, unless otherwise stated, cells were treated wit h 100 μM TA to investigate its browning effect. As shown in Fig. 1C, TA significantly up-regulated expression of BAT signature proteins (PGC-1α, PRDM16, and UCP1) in a dose-dependent manner (Fig. 1C) as well as thei r encoding genes (*Ppargc1a*, *Prdm16*, and *Ucp1*) and beige-specific genes, including *Cd137*, *Cited1*, *Tbx1*, and *Trem26* (Fig. 1D). Recruitment of beige cells in 3T3-L1 adipocytes consequently led to reduced fat accumulation, as evidenced by reduced triglycerides after TA treatment (Fig. 1E).

## 3.2 TA treatment alleviates HFD-induced obesity in mice

Based on the positive results obtained *in vitro*, we tested the anti-obesity effects of TA in HFD-induced obese mice. Daily oral administration of 100 mg/kg of TA to HFD-fed mice for 8 weeks dramatically reduced body weight gain (27.3% reduction compared to HFD-fed controls) (Fig. 2A). TA reduced WAT weight of obese mice and food efficiency but elevated BAT fat mass (Fig. 2B, C). To confirm the browning effects of TA in inguinal WAT (iWAT) of mice, expression levels of brown fat-specific genes and proteins were determined. As shown in Fig. 2D, E, expression levels of key brown adipocyte and beige-specific genes (*Ppargc1a*, *Prdm16*, and *Ucp1* as well as *Cd137*, *Cited1*, *Tbx1*, and *Tmen26*) were up-regulated upon TA treatment. Histological observation by H&E staining also indicated reduction of both adipocyte size and

recruitment of beige adipocytes in iWAT (Fig. 2F). Skin temperature measured using a thermal imaging camera was elevated in the TA-treated group compared to the control counterparts (Fig. 2G), implying increased thermogenic activity.

### 3.3 TA regulates lipid metabolism in white adipocytes

We next investigated whether TA affects lipid metabolism in white adipocytes. Firstly, we determined protein expression levels of three important adipogenic markers, including C/EBPα, PPARα, and PPARγ, in iWAT. Expectedly, their expression levels were reduced upon TA treatment, suggesting reduction of adipogenesis (Fig. 3A). Moreover, expression of important lipogenic markers, acetyl-CoA carboxylase (ACC) and fatty acid synthase (FAS), was markedly reduced upon TA treatment with an increased ratio of pACC to total ACC mediated by AMPK activation (Fig. 3B). Next, we investigated expression levels of lipolysis-related proteins, including hormone sensitive lipase (HSL) and adipocyte triglyceride lipase (ATGL), before and after TA treatment. As shown in Fig. 3C, TA enhanced lipolysis by increasing expression of HSL and ATGL. TA treatment also led to significant elevation of mitochondrial protein levels of acyl-coenzyme A oxidase 1 (ACOX1) and carnitine palmitoyltransferase 1 (CPT1), suggesting augmented oxidative capacity upon TA treatment (Fig. 3D).

### 3.4 TA increases mitochondrial biogenesis in white adipocytes

TA increased mitochondrial biogenesis in iWAT, as determined by elevated expression of genes (*Cox4*, *Nrf1*, *MtDNA*, and *Tfam*) responsible for mitochondrial biogenesis (Fig. 4A). Indeed, staining of differentiated adipocytes with MitoTracker green revealed stronger signals in TA-treated adipocytes compared to the control (Fig. 4B). Increased mitochondrial biogen

esis upon TA treatment was also validated by transmission electron micros copy, which showed elevated mitochondrial numbers in iWAT of TA-treate d mice (Fig. 4C).

### 3.5 TA activates brown adipocytes

Next, we investigated whether TA influences brown adipocyte activ ity by determination of expression levels of brown fat-specific marker prot eins and genes (*Cidea, Eva1, Lhx8, Ppargc1a, Prdm16, Ucp1,* and *Zic1*). As shown in Fig. 5, TA significantly up-regulated key brown fat markers (Fig. 4D) and genes (Fig. 4E) in BAT of TA-treated mice. H&E-stained B AT images also support these results, showing reduction of lipid droplet fo rmation in TA-treated mice (Fig. 4F). ICC staining also revealed an increa sed signal in BAT treated with TA compared to the control (Fig. 4G).

### 3.6 Molecular docking analysis

Comparative analysis of docking scores among the protein targets responsible for browning was carried out to select the best target protein. Protein showing the lowest binding energy in its interaction with TA was considered to be the best possible target for molecular interaction. Accordin g to the docking analysis, SIRT1 displayed a binding energy of -21.25 (KJ /mol) and a G-score of -5.08 (Kcal/mol) as well as the strongest binding affinity of -35.097 KD with TA, although a good binding energy of -13.68 (KJ/mol) and G-score of -3.27 (Kcal/mol) were observed for β3-AR (Tabl e 2). The binding positions of TA with each protein were evaluated to con firm the best binding protein (Supplementary Fig. 2-6). We considered the best position to be those displaying binding at the protein  active site. The 2-D interaction diagram shows strong hydrogen bond formation of TA wit h tyrosine 280 residue of SIRT1 based on a distance of only 1.89 Å (Fig.

5A-D). This result confirms a correlation with the reported active site residues for SIRT1. The predicted active site for SIRT1 showed efficient binding with TA, representing a significant conformational change in SIRT1 protein. In the case of β3-AR, a hydrogen bond was formed by the residue alanine 311 with a distance of 1.93 Å. However, unlike the SIRT1 interaction, TA did not bind to the active site of the receptor membrane protein (Fig. 5E-H).

### 3.7 TA induces browning of white adipocytes via activation of β3-AR and regulation of AMPK-mediated SIRT1

We next investigated molecular mechanisms behind the browning activity of TA. To this end, we separately treated cells with β3-AR antagonist (L-748.337, 20 μM) and agonist (BRL 37344, 20 μM) with or without TA (100 μM) for 7 days of differentiation, after which expression levels of key signaling molecules responsible for browning (UCP1, PRDM16, PGC-1α, and PKA) were determined. Inhibition of β3-AR by antagonist resulted in reduced expression of UCP1, PRDM16, PGC-1α, and PKA, whereas agonist up-regulated expression of PKA and browning markers (Fig. 6A). Interestingly, after performing molecular docking, TA showed strong binding at the active site of SIRT1. Consequently, we determined the expression levels of lipid-metabolizing signaling molecules (UCP1, PRDM16, PGC-1α, AMPK, and pAMPK) after separate treatment of 3T3-L1 cells with SIRT1 antagonist (EX527, 40 μM) and agonist (resveratrol, 40 μM) after 7 days of differentiation. TA activated AMPK by increasing the ratio of AMPK to pAMPK. Inhibition of SIRT1 by antagonist caused reduced expression of UCP1, pAMPK, PRDM16, and PGC1-α, whereas agonist caused increased expression of browning markers (Fig. 6B). This indicates that SIRT1 also had a direct effect on the mechanism of browning and elevated thermogenesis along with β3-AR in white adipocytes.

Table 1. Primer sequences used for real-time quantitative RT-PCR.

| Gene | Forward | Reverse |
|---|---|---|
| *Cd137* | GGTCTGTGCTTAAGACCGGG | TCTTAATAGCTGGTCCTCCCTC |
| *Cidea* | CGGGAATAGCCAGAGTCACC | TGTGCATCGGATGTCGTAGG |
| *Cited1* | GGGGTAAAAGATCGCAAGGC | TGGTAGAAGGGGTGGCAGTA |
| *Cox4* | TGACGGCCTTGGACGG | CGATCAGCGTAAGTGGGGA |
| *Eva1* | AGTGCTGATAAAGCCGAGGG | AGCTTCTCGAAGTGTTAGTCTGT |
| *Lhx8* | CATCGCTGTTCTGCCTGTTAG | CTCGGGATTCAGCAGTCCTTC |
| *MtDNA* | CCGTCACCCTCCTCAAATTA | GGGCTAGGAGTTCAGAGTG |
| *Nrf1* | GCTAATGGCCTGGTCCAGAT | CTGCGCTGTCCGATATCCTG |
| *Ppargc1a* | ATGAATGCAGCGGTCTTAGC | AACAATGGCAGGGTTTGTTC |
| *Prdm16* | GATGGGAGATGCTGACGGAT | TGATCTGACACATGGCGAGG |
| *Tbx1* | AGCGAGGCGGAAGGGA | CCTGGTGACTGTGCTGAAGT |
| *Tfam* | ATGTGGAGCGTGCTAAAAGC | GGATAGCTACCCATGCTGGAA |
| *Tmem26* | GAAACCAGTATTGCAGCACCC | CCAGACCGGTTCACATACCA |
| *Ucp1* | CCTGCCTCTCTCGGAAACAA | GTAGCGGGGTTTGATCCCAT |
| *Zic1* | GCCACAAATCCGGGAAGAAG | CTCACTTTCTCGCCGCTCAG |

Table 2. Binding energies for different regulatory proteins involved in lipid metabolism and browning, interactions with *trans*-anethole, and the degree of conformational change after binding.

| Proteins | Best[1] Pose | Binding energy (KJ/mol) | G-score[2] (Kcal/mol) | Binding Affinity (kD) | Cluster[3] RMSD | Reference[4] RMSD |
|---|---|---|---|---|---|---|
| SIRT1 | 17 | -21.25 | -5.08 | -35.097 | 0.89 | 14.93 |
| PKA | 7 | -14.85 | -3.55 | -26.023 | 0.69 | 8.36 |
| β3-AR | 14 | -13.68 | -3.27 | -31.931 | 0.44 | 9.42 |
| p38 | 5 | -10.08 | -2.41 | -22.023 | 0.25 | 5.35 |
| ERK2 | 17 | -10.08 | -2.41 | -15.093 | 0.52 | 11.23 |
| ERK1 | 4 | -9.62 | -2.3 | -19.913 | 0.43 | 6.18 |
| AMPK | 4 | -8.95 | -2.14 | -24.087 | 0.17 | 6.2 |

[1] Best binding position; [2] Glide-score for calculating binding energy; [3] Root Mean Square Difference between input structure and after formation of cluster; [4] Root Mean Square Difference between the reference structure and the input structure

Supplementary Table 1. Descriptive properties of selected target proteins for molecular docking.

| Protein name | UniProt ID | PDB ID | Chain[1] | Length[2] | Gene[3] | Classification [4] |
|---|---|---|---|---|---|---|
| AMPK | P54646 | 2H6D | A | 276 | PRKAA2 | Signalling Protein, Transferase |
| ERK1 | P27361 | 2ZOQ | A,B | 382 | MAPK3 | Transferase |
| ERK2 | P28482 | 1TVO | A | 368 | MAPK1 | Transferase |
| p38-MAPK | Q16539 | 3DS6 | A,B,C,D | 366 | MAPK14 | Transferase |
| PKA | P17612 | 3L9L | A,B | 351 | PRKACA | Transferase/ Transferase Inhibitor |
| SIRT1 | Q96EB6 | 4I5I | A,B | 287 | SIRT1 | Hydrolase |
| β3-AR | P13945 | 2CDW | A | | ADRB3 | Membrane receptor |

[1] Total number of subunits present in the protein; [2] Total length of all the su bunits in the protein; [3] Gene encoding for the protein; [4] Family of protein

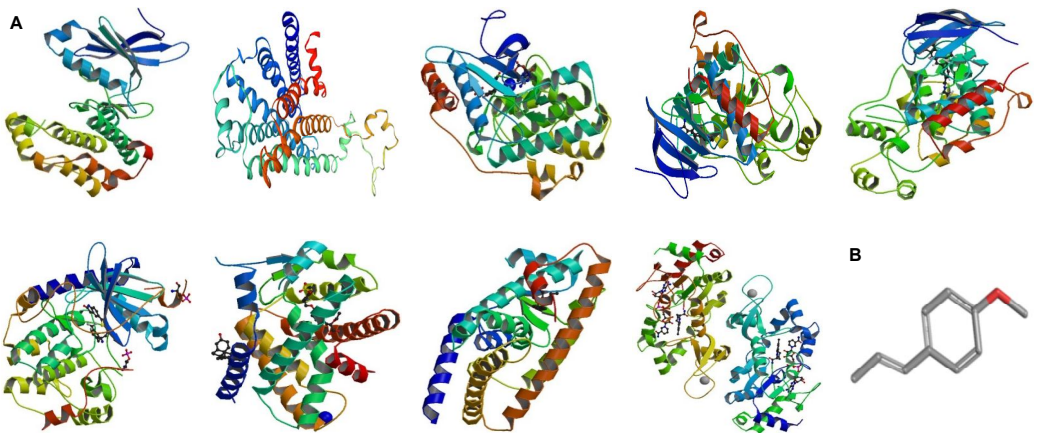


Supplementary Fig. 1. Enlisted structures of proteins utilized for docking in the following order (left to right): AMPK, β3-AR, ERK1, ERK 2, p-38 MAPK, PPARα, PPARɣ, SIRT1 (A); 3-D crystal structure of ligand-based compound *trans*-anethole (B).

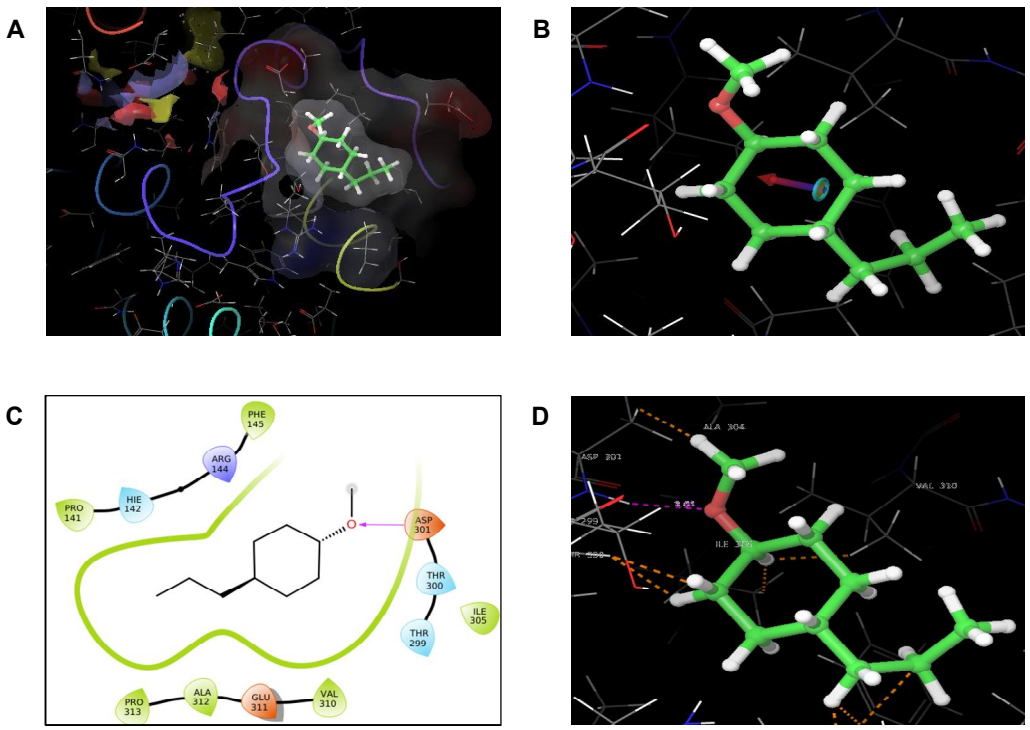


Supplementary Fig. 2. Molecular docking of PKA with TA at the active site but comprising weak binding (A); Polar interaction of ligand with PKA (B); 2-D interaction diagram after complete do cking displaying pi-pi interaction and hydrogen donation by residue Aspartate 301 (C); Hydrogen bond distance of 2.01Å (D).

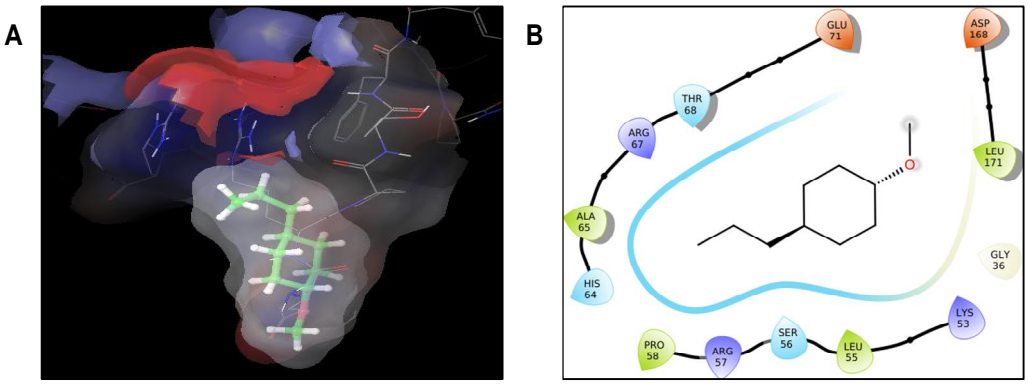


Supplementary Fig. 3. Molecular docking of p-38 with TA at active site but with weak binding in the absence of any hydrogen bonding (A); 2-D interaction diagram after complete docking (B).

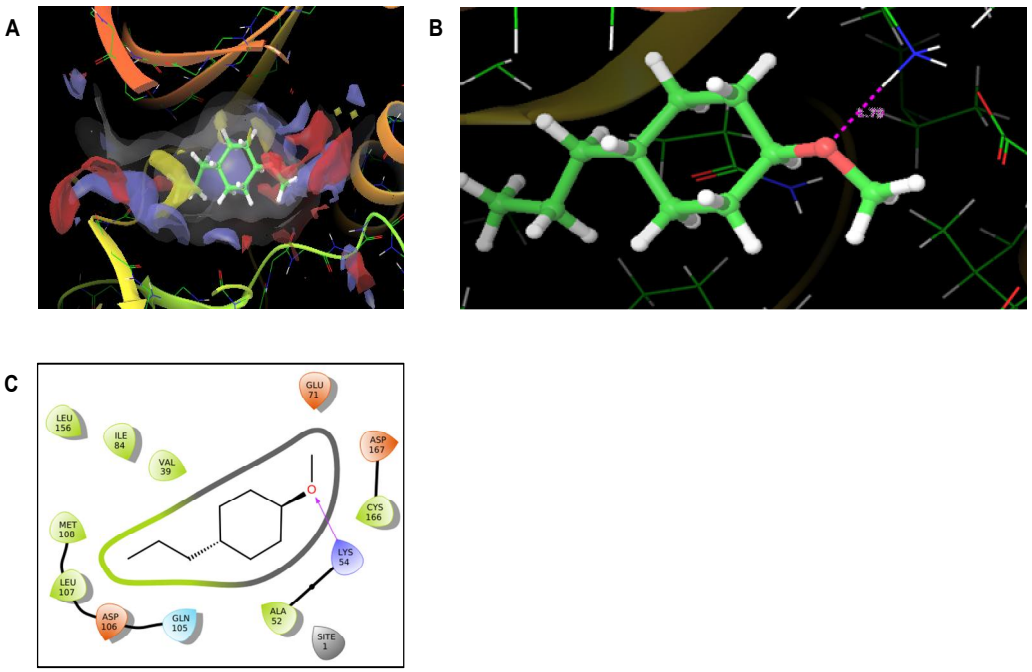


Supplementary Fig. 4. Molecular docking of ERK2 with TA at active site with moderate binding (A); Hydrogen bond distance of 1.79Å (B); 2-D interaction diagram after complete docking displaying hydrogen donation by residue Lysine 54 (C).

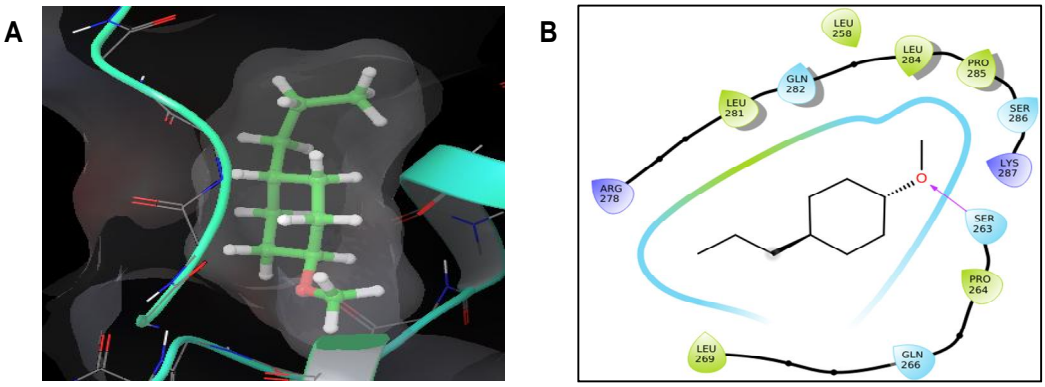


Supplementary Fig. 5. Molecular docking of ERK1 with TA with very weak binding in the absence of any hydrogen bonds (A); 2-D interaction diagram after complete docking (B).

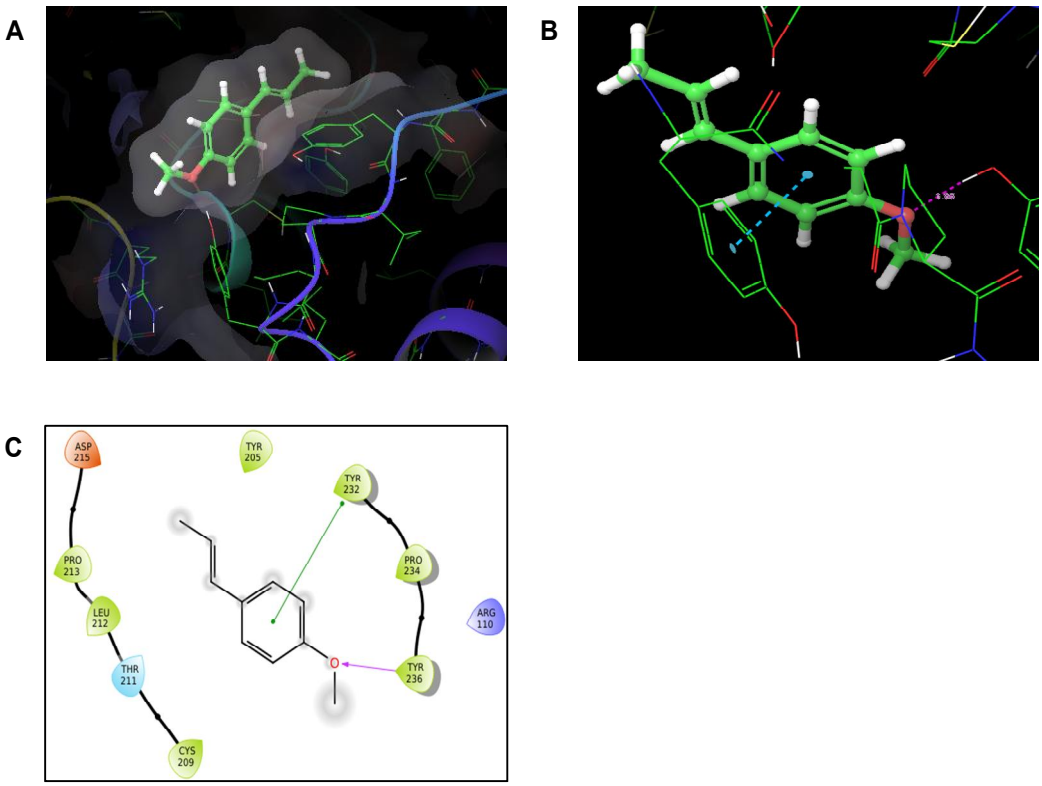


Supplementary Fig. 6. Molecular docking of AMPK with TA (A); Polar interactions and hydrogen bond distance of 1.36 Å (B); 2-D interaction diagram after complete docking displaying pi-pi interaction and hydrogen donation by residue Tyrosine 232 (C).

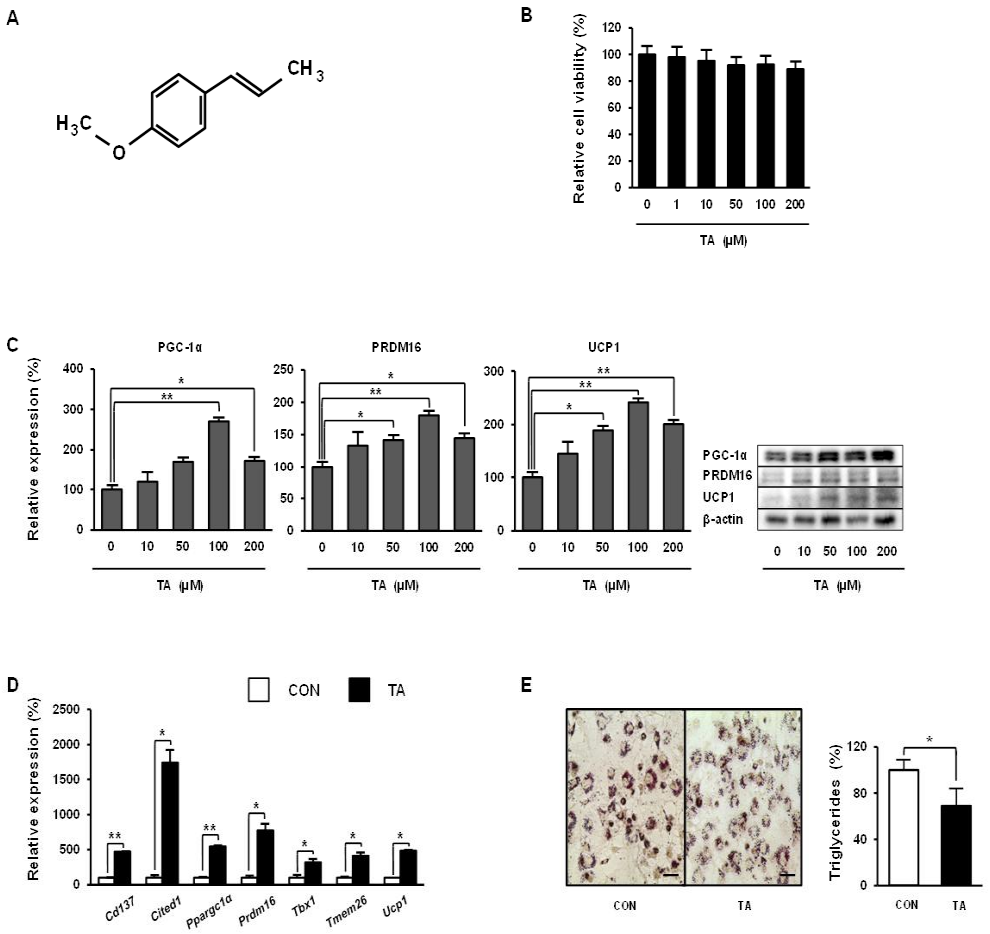


Fig. 1. *Trans*-anethole (TA) induces browning in 3T3-L1 white adipocytes.

Chemical structure of *trans*-anethole (A) and cytotoxicity (B). TA promotes expression of core brown fat marker proteins (C) in a dose-dependent manner as well as beige fat-specific genes (D) at 100 μM in 3T3-L1 adipocytes. Representative images of Oil Red O staining of 3T3-L1 were taken at X20 magnification (scale bars= 50 μm), where lipid content was quantified by extracting Oil Red O stain bound to cells with 100% isopropanol in 3T3-L1 adipocytes (E).Data are presented as the mean ±S.D., and differences between groups were determined using the Statistical Package of Social Science (SPSS, version 17.0; SPSS Inc., Chicago, IL, USA) program, followed by Tukey's post-hoc tests or Student's t-test. Statistical significance between control and TA-treated mice is shown as $^{*}p < 0.05$ or $^{**}p < 0.01$.

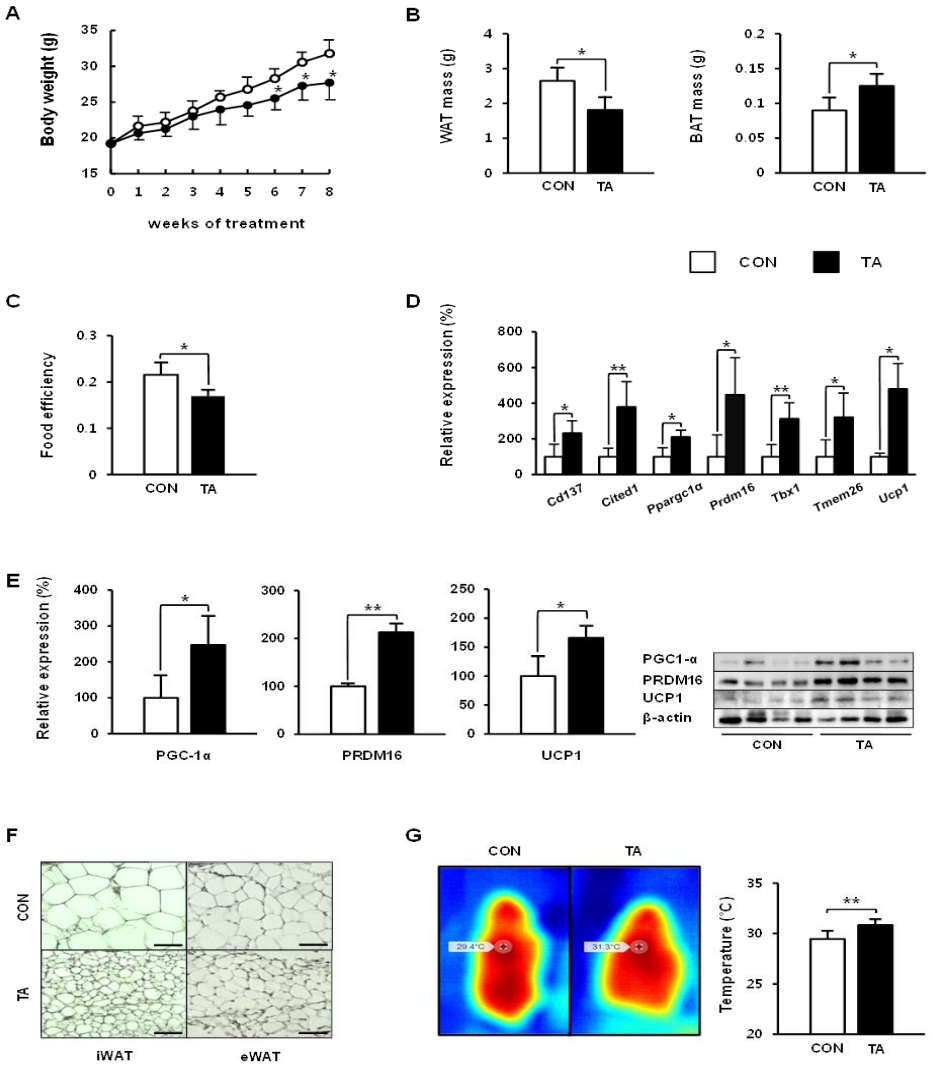


Fig. 2. *Trans*-anethole (TA) protects obesity by browning of white fat in obese mice fed a high fat diet.

Effects of TA treatment on body weight gain (A), WAT and BAT mass (B), food efficiency (C), expression of beige fat-specific marker genes (D) and proteins (E), induction of beige fat cells in inguinal white adipose tissues (F)(scale bars=50 μm), and skin temperature (G). TA (100 mg/kg body weight) was administered daily. Data are presented as the mean ±S.D., and differences between groups were determined using the Statistical Package of Social Science (SPSS, version 17.0; SPSS Inc., Chicago, IL, USA) program, followed by Tukey's post-hoc tests or Student's *t*-test. Statistical significance between control and TA-treated mice is shown as $^{*}p < 0.05$ or $^{**}p < 0.01$.

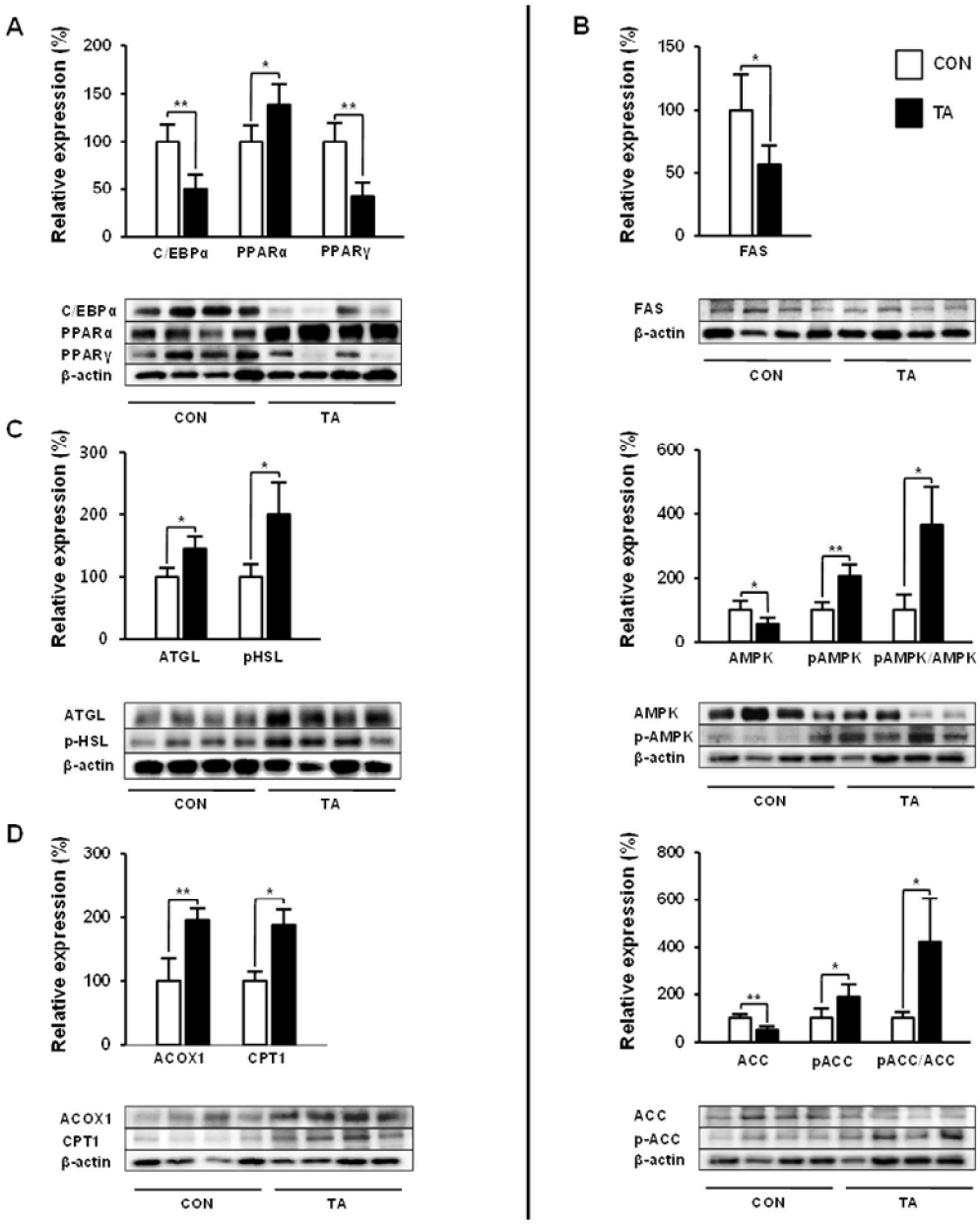


Fig. 3. *Trans*-anethole (TA) regulates lipid metabolismin white adipose tissue.

TA regulates lipid metabolic regulators involved in adipogenesis (A), lipogenesis (B), lipolysis (C), and fatty acid oxidation (D). Data are presented as the mean ± S.D., and differences between groups were determined using Student's *t*-test. Stati stical significance between control and TA-treated mice is shown as $^{*}p < 0.05$ or $^{**}p < 0.01$.

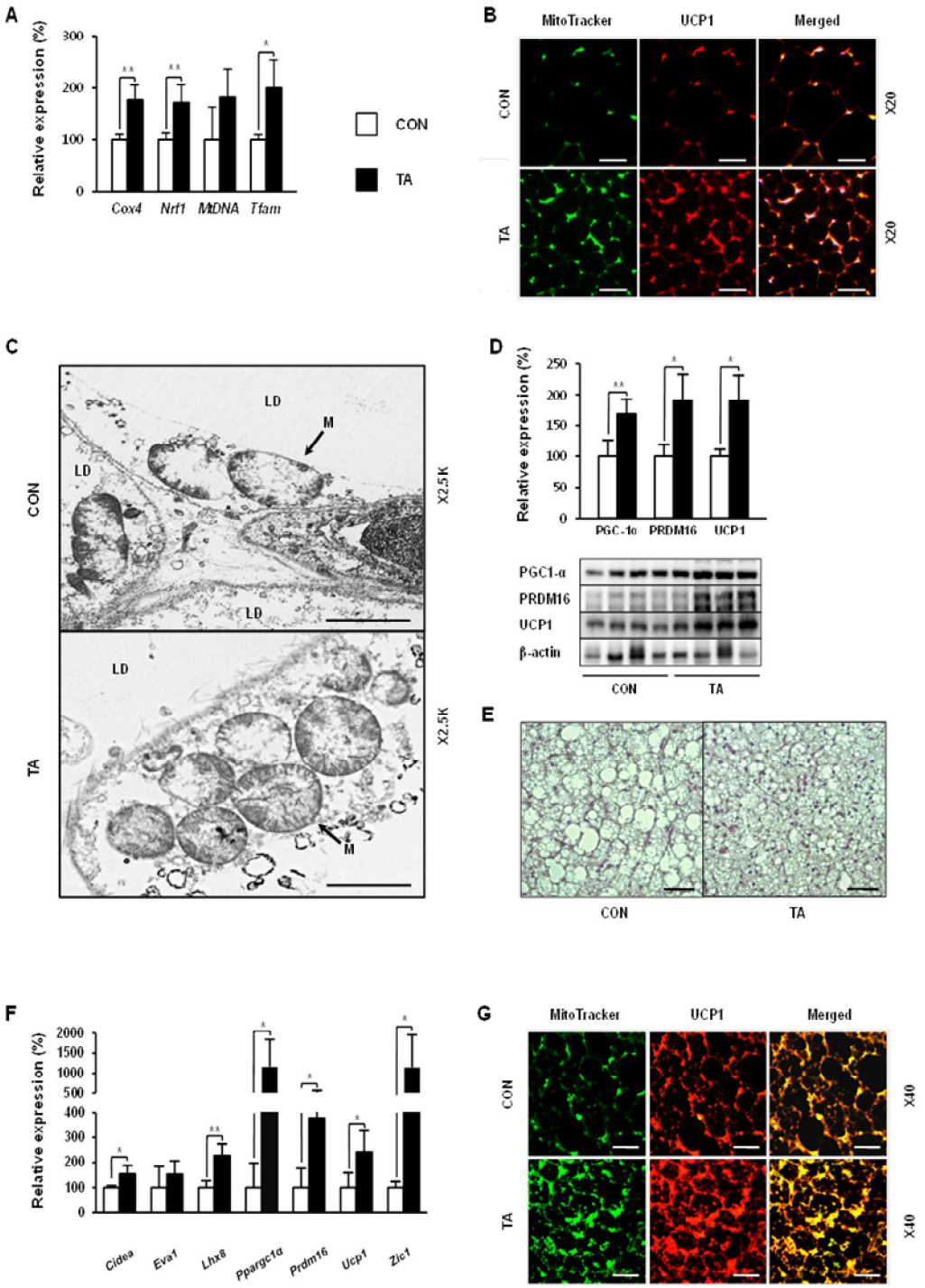
A
Relative expression (%)
300
200
100
0
Cox4
Nrf1
MtDNA
Tfam
CON
TA
B
MitoTracker
UCP1
Merged
CON
TA
X20
X20
C
CON
TA
LD
M
X2.5K
X2.5K
D
Relative expression (%)
250
200
150
100
50
0
PGC-1α
PRDM16
UCP1
PGC1-α
PRDM16
UCP1
β-actin
CON
TA
E
CON
TA
F
Relative expression (%)
2000
1500
1000
500
400
300
200
100
0
Cidea
Eva1
Lhx8
Ppargc1α
Prdm16
Ucp1
Zic1
G
MitoTracker
UCP1
Merged
CON
TA
X40
X40

Fig. 4. *Trans*-anethole (TA) elevates mitochondrial biogenesis and activates brown adipocytes.

TA increasesmitochondrial biogenesis in iWAT of HFD-fed mice by up-regulating expression of genes responsible for mitochondrial biogenesis (A). ICC staining of differentiated adipocytes withMitoTracker Green (scale bars= 50μm) for UCP1, where the images were captured at 20X magnification (B). Transmission electron microscopic images of iWAT of control and TA-treated mice, where the images were captured at X2.5k magnification (C) (scale bars=2μm), where LD means lipid droplet, M refers to mitochondrion with arrows, and N stands for nucleus. *Trans*-anethole (TA) activates brown adipocytes by increasing expression of key brown-fat markers (D) and genes (E) in BAT of TA-treated mice. Representative histological sections of BAT stained with hematoxylin and eosin (H&E) (scale bars=50μm) (F). ICC staining of differentiated BAT with MitoTracker Green (scale bar=20$\mu$m) for UCP1, where the images were captured at X40 magnification (G). Data are presented as the mean ±S.D., and differences between groups were determined using Student's *t*-test. Statistical significance between control and TA-treated mice is shown as $^{*}p < 0.05$ or $^{**}p < 0.01$.

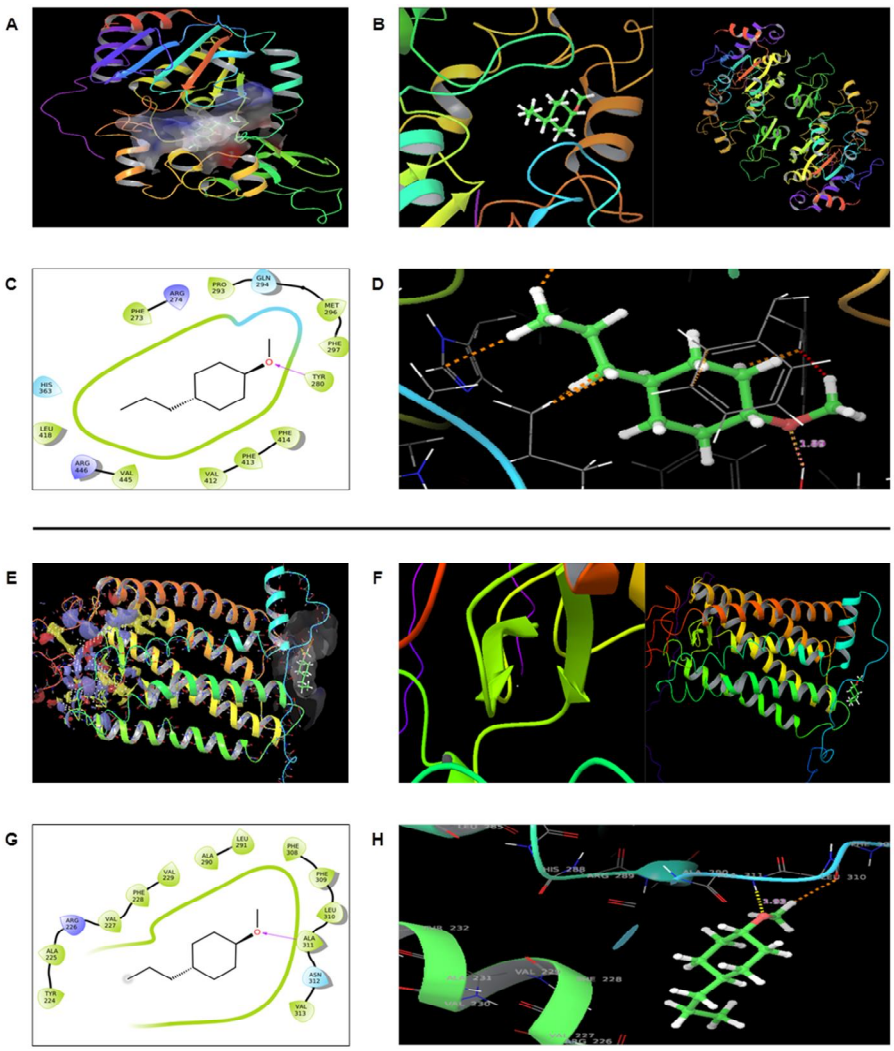


Fig. 5. Molecular docking of *trans*-anthole (TA) with Sirtuin1 and β3-adrenergic receptor protein.

TA binds to the active site domain of SIRT1 (A), and visualization of ligand TA binding after complete docking with chain A of protein (B). 2-D interaction diagram of TA forming hydrogen bond with residue Tyrosine280 (C) with a distance of 1.89Å (D). TA does not bind to the active site domain of β3-AR (E), and the visualization of ligand TA binding after complete docking with chain A of the receptor protein (F). 2-D interaction diagram of TA forming hydrogen bond with residue Alanine 311 (G) with a distance of 1.93Å (H). Data presented as per the results obtained from Glide docking (Schrödinger Release 2017-4: Glide, 2017).

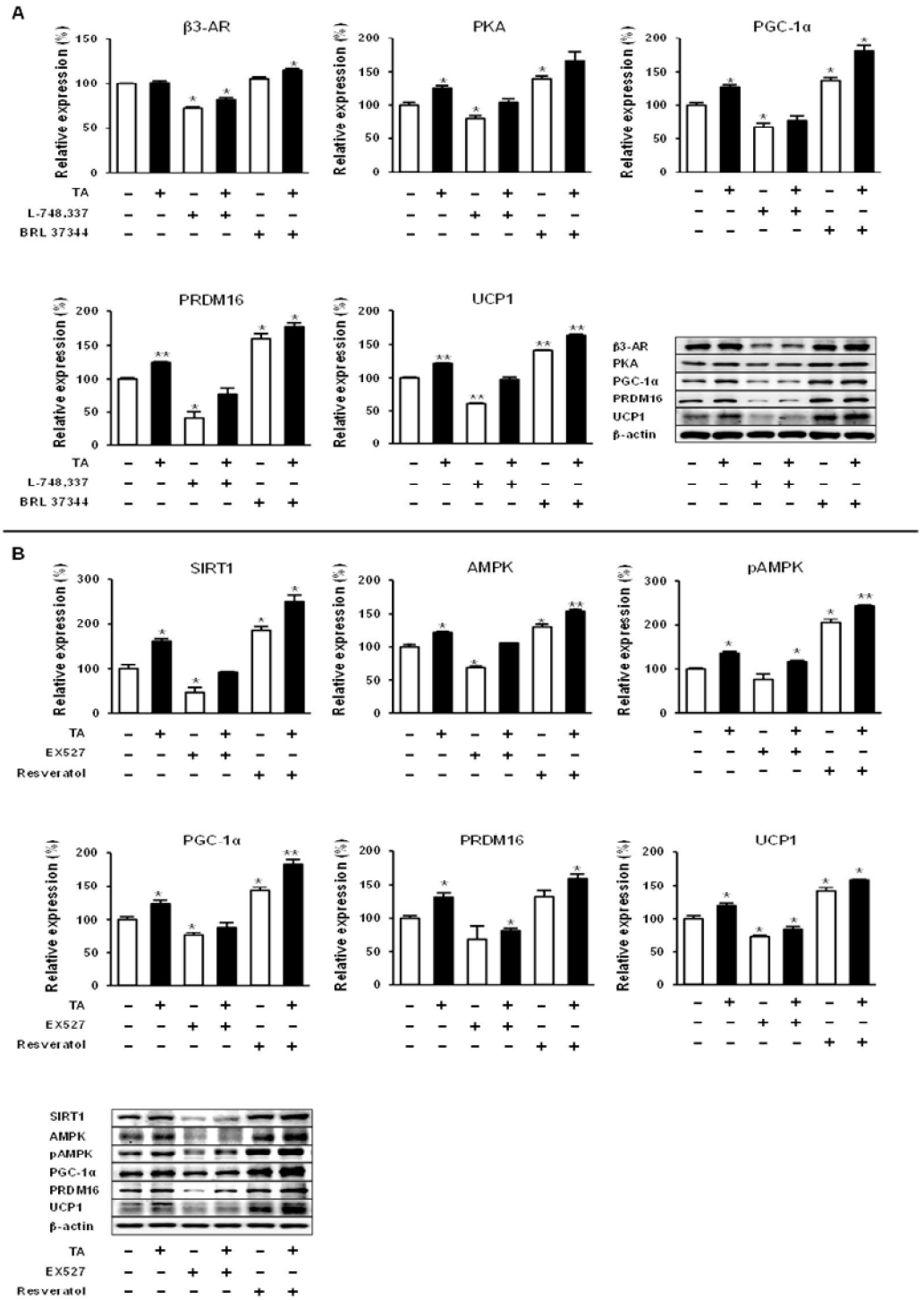
A
β3-AR
PKA
PGC-1α
PRDM16
UCP1
Relative expression (%)
TA
L-748,337
BRL 37344
β3-AR
PKA
PGC-1α
PRDM16
UCP1
β-actin
B
SIRT1
AMPK
pAMPK
PGC-1α
PRDM16
UCP1
Relative expression (%)
TA
EX527
Resveratol
SIRT1
AMPK
pAMPK
PGC-1α
PRDM16
UCP1
β-actin

Fig. 6. Induction of browning via *trans*-anethole (TA) following β3-AR as well as SIRT1 pathway in 3T3-L1 adipocytes.

TA activates β3-AR by elevating expression of PKA and promotes browning by elevating expression of browning markers PGC-1α, PRDM16, and UCP1 (A) as well as SIRT1-mediated activation of AMPK to pAMPK, resulting in higher expression levels of browning markers (B) in comparison to the effect of β3-AR. Data are presented as the mean ±S.D., and differences between groups were determined using the Statistical Package of Social Science (SPSS, version 17.0; SPSS Inc., Chicago, IL, USA) program, followed by Tukey's post-hoc tests. Statistical significance between control and TA-treated mice is shown as $^{*}p < 0.05$ or $^{**}p < 0.01$.

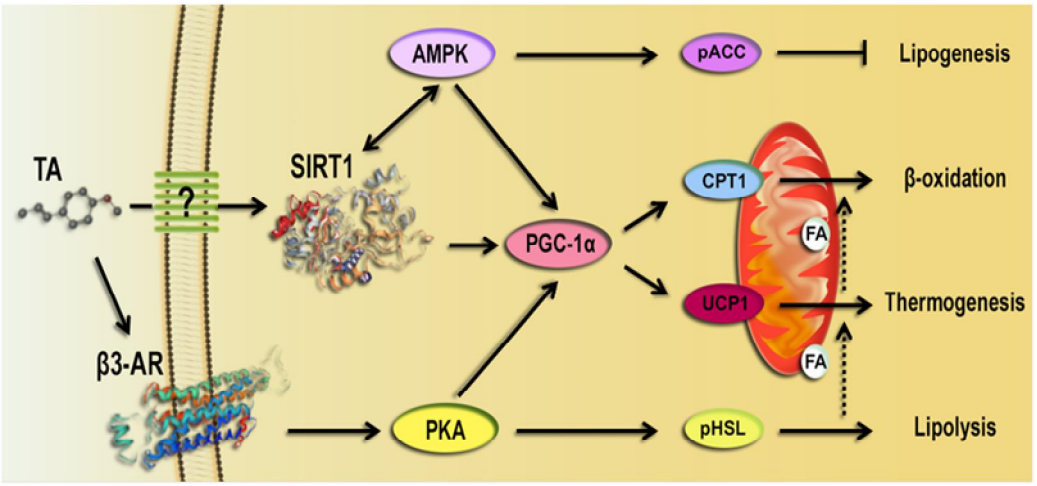


Fig. 7. Suggested pathway for TA-induced browning via β3-AR and AMPK-mediated SIRT1 pathway.

# 4. Discussion

The present study explored the possible use of TA, abundantly present in plant oils, as an anti-obesity candidate. We observed its potential capability to induce the brown fat-like phenotype in cultured white adipocytes and in inguinal WAT of diet-induced obese mice. Plant- derived essential oils are rich sources of volatile organic compounds, and some have been known to have anti-obesity properties (Rashed et al., 2017). Anti-obesity effects of essential oils are mediated through several possible molecular mechanisms, including anti-adipogenesis and anti- lipolysis (Quiroga et al., 2013; Lee et al.,2011). Moreover, earlier reports demonstrated that olive oil can cause increased oxygen consumption and expression of UCPs in BAT. For example, olive oil feeding up-regulates UCPs in rat BAT and skeletal muscle, thereby increasing thermogenic capacity (Rodriguez et al., 2002). Olive oil also stimulates secretion of norepinephrine and adrenaline, which are major thermogenic signaling molecules, whereas phenolic compounds such as oleuropein and its derivatives play a major role in the regulation of thermogenesis (Oi-Kano et al., 2016).

Recently, it was reported that curry oil containing TA as a major component has an appetite-enhancing effect in mice (Ogawa et al., 2016). In contrast, fennel tea containing TA (3.1%) was shown to suppress appetite in overweight women (Bae et al., 2015). It is still in doubt which components may contribute to the efficacy of appetite control. Due to its low water solubility, strong odor, high rate of vaporization, and lower stability of its physiochemical state, TA has limited applications (Zhang et al., 2015). Oral administration of TA may be more recommended since it is completely absorbed and its metabolites generated by hepatic biotransformation are responsible for its anti-inflammatory effects, which are greater than those of T

A itself (Freire et al., 2005). In this study, we applied 100 mg/kg of TA b ased on data from antecedent research on chronic toxicity in rats (Truhaut et al., 1989), and this dose of TA is known to be extensively absorbed, me tabolized, and eliminated in rodents (Sangster et al., 1984). The major route of metabolism of TA in rodents is via oxidative *O*-demothylation, and this metabolic route is similar to that of humans (Sangster et al., 1984). TA w as accorded with Generally Recognized as Safe status by the Food and Dr ug Administration and the Flavors and Extracts Manufacturer's Association (Hall et al., 1968). The only effects observed were slight hepatic changes a t a high dose of 500~ 700 mg/kg as well as depicted reports with apparent retardation of body weight gain and transient clinical features such as anor exia and lethargy depicting a protective hepatotoxic effect of TA on anti-i nflammatory cytotoxicity (Truhautetal.,1989). As observed in our study, slig ht intake of 100 mg/kg of TA exhibited substantial reduction of body weig ht gain in the case of diet-induced obese mice subjects, confirming the ant i- obesity effect of TA.

In the case of adipogenesis, transcription factor C/EBPα accompanied with PPARγ is responsible for growth arrest in the early stages of adipocy te differentiation. PPARγ expression is considered as a major checkpoint fo r the regulation of adipocyte lipid synthesis by increasing lipogenic gene (F AS and ACC) expression via activation of AMPK (Tung et al., 2017). Simi larly, in our study, we observed down-regulation of C/EBPα as well as PP ARγ as well as elevated levels of pACC to ACC mediated by AMPK activ ation. This implies a notable decrease in adipogenesis and lipogenesis. We also observed up-regulation of HSL, ATGL, ACOX1, and CPT1, essential marker proteins, upon TA treatment, demonstrating enhanced lipolysis and mitochondrial biogenesis. Identical results in other reports (Saponaro et al., 2015; Rupasinghe et al., 2016) provide supporting evidence.

The molecular mechanism mediated by TA in the induction of browning can be revealed based on expression of β3-AR and SIRT1 through *in vitro* as well as *in silico* analysis. We observed abolished expression of core browning proteins such as UCP1, PRDM16, and PGC-1α when AMPK was inhibited in brown adipocytes in the presence of TA, implicating AMPK and PGC-1α in the browning mechanism. Corresponding studies have reported that AMPK-independent phosphorylation of ACC for BAT thermogenesis is by fatty acid oxidation and activation of AMPK by β3-adrenergic stimuli play important roles in mitochondrial structural and functional maintenance and quiescence as well in brown and beige adipose tissues (Motillo et al., 2016; Gonzalez-Hurtado et al., 2018). Additionally, this theory led us to test the hypothesis regarding the connection between PKA and AMPK. We obtained positive and significant results, as pAMPK and AMPK levels increased upon TA treatment, followed by possible up-regulation of thermogenic markers (UCP1, PRDM16, and PGC-1α). However, this effect was forfeited by treatment with AMPK antagonist. In a similar manner, TA exhibited an agonistic effect along with SIRT1 by enhancing PPARα and PGC-1α in 3T3-L1 adipocytes to promote energy expenditure (Collins et al., 2011).

Moreover, many studies have demonstrated the use of efficient and time-saving techniques such as molecular docking to categorize and specify target compounds and proteins. Recent reports have demonstrated structure-based screening of potential compounds for determination of active drugs, whereas a different study characterized regulatory proteins to determine expression of specific inhibitory compounds on the basis of molecular docking and dynamics (Singh et al., 2017; Bhattacharjee et al., 2015). Similarly, based on the docking results, we selected the best target protein for TA that attenuated the strong binding effect of TA to SIRT1 in comparison to other browning and lipid-metabolizing proteins.

AMPK activates PGC-1α through direct phosphorylation and by facil

itating SIRT1-dependent PGC-1α deacetylation and promotes oxidative me tabolism in several metabolic tissues, playing a critical role in regulating e nergy state of cells (Weikel et al., 2016). However, the effect of AMPK o n UCP1 expression in WAT remains unclear and is known to be species-d ependent (Bonet et al., 2014). APMK activator agonists such as AICAR inc rease $NAD^+$ levels and SIRT1 activity. There is evidence that SIRT1 protei n represses PPARγ activity in 3T3-L1 adipocytes, there by attenuating ad ipogenesis and potentiates the response of β3-AR stimuli to enhance BAT function (Boutant et al., 2015; Rahmanetal., 2011). Moreover, lipolysis is tri ggered in the case of SIRT1 up-regulation in differentiated fat cells, and induction of mitochondrial biogenesis is possible via regulation of PGC-1α by SIRT1 protein (Boutantetal., 2015; Wangetal.,2013).

In conclusion, TA possesses potential therapeutic implications for the treatment of obesity by playing multiple modulatory roles in the induction of white fat browning, activation of brown adipocytes, and promotion of lip id catabolism. Collective data of molecular mechanism study and molecular docking analysis revealed that TA induced browning of 3T3-L1 adipocytes through activation of β3-AR as well as the AMPK-mediated SIRT1 pathw ay regulating PPARα and PGC-1α (Fig. 7).

# CHAPTER 2

# *Trans*-Cinnamic Acid Stimuqlates White Fat Browning and Activates Brown Adipocytes

# 1. Introduction

Obesity is associated with numerous other metabolic complications including diabetes, hypertension, hyperlipidemia, atherosclerosis, and cardiovascular diseases (Mnafgui et al., 2015). Notably, obesity is caused by oversupply of energy provided by excess fat that is accumulated in the body without being consumed (Lei et al., 2007). Besides exercise and calorie restriction, another alternative way to lose weight and reduce obesity is to increase energy expenditure by activating brown adipocytes (Tan et al., 2011).

There are three types of fat in humans: 1. white adipose tissue (WAT) which makes up nearly all fat in adults; 2. brown adipose tissue (BAT) that is involved in energy expenditure; and 3. brown in white fat (brite or beige fat) which converts from white adipocytes to brown-like adipocytes and contributes to energy expenditure in humans (Carey et al., 2014). Targeting adipose tissue has potential therapeutic importance for the treatment of obesity and other metabolic disorders (Jang et al., 2018). Recent discovery of brown fat in human adults has heightened interest in research of beige adipocytes toelevatethermogenicprograminentireadipocytes(Claussnitzereta l.,2015;Leeetal.,2016).

The fundamental factor leading to the process of adaptive thermogenesis is governed by uncoupling protein 1 (UCP1) (Sellayah et al., 2014) known to be expressed in brown and beige adipocytes (Lim et al., 2012). UCP1 releases heat as a form of energy after uncoupling the electron transport chain for energy production (Ricquier et al., 2011). It plays a critical role in energy balance and metabolic regulation of cold and diet-induced thermogenesis (Azzu et al., 2010; Parray et al., 2017). Recent studies have identified ectopic expression of other hallmark proteins such as PGC-1α and PRDM16 as novel beige-fat-specific markers (Tiraby et al., 2003; Sharp et al., 2012). These proteins can be targets for the identification of brown fat-activat

ion or browning/beiging agents (Lee et al., 2014; Fisher et al., 2012; Seale et al., 2011). Among the genetic markers *Cd137, Cited1, Tbx1,* and *Tmem26* has been reported for beige-specific markers while genes *Eva1, Lhx8* and *Zic* have been specified for brown adipocytes (Harms et al., 2013; Barquissau et al., 2016).

Recently, advances have been made to understand the roles of pharmacological agents and dietary supplements that contribute to browning of white adipocytes (Bonet et al., 2018). To date, a variety of natural compounds have shown promise for regulating BAT activity and recruiting beige adipocytes as well as enhancing lipolytic and catabolic potential of WAT (Bonet et al., 2018; Azhar et al., 2016; Kang et al., 2018; Lone et al., 2017).

Cinnamon (*Cinnamomum cassia*) is one of the most important spices used daily by many people all over the world. Cinnamon primarily contains vital oils (*C vernum*) and other derivatives such as cinnamaldehyde and cinnamic acid (Barceloux et al., 2009; Rao et al., 2014). Among several analogs of cinnamon, *trans*-cinnamic acid (*t*CA) is known to exhibit various health-promoting properties, including anti-diabetic (Anderson et al., 2014), anti-inflammatory, and anti-cancer activities (Soliman et al., 2012). Another important feature displayed by *t*CA is that it can reduce body weight of obese rats (Jain et al., 2017) by improving insulin sensitivity and blood lipids (Kopp et al., 2014).

To date, little research has been done concerning regulatory roles of *t*CA in lipid metabolism, particularly in fat browning. Therefore, the objective of the present study was to examine physiological roles of *t*CA in lipid metabolism of 3T3-L1 white adipocytes and HIB1B brown adipocytes, focusing on browning.

## 2. Materials and methods

### 2.1 Chemicals

*Trans*-cinnamic acid (99% purity, Fig. 8A) was purchased from Sigma Chemical Co. (St. Louis, MO, USA). BRL 37344 and L-748.337 were purchased from Tocris Bioscience (Bristol, UK). AICAR was purchased from TCI (Chuo-ku, Tokyo, JAPAN). Dorsomorphin was purchased from Abcam (Cambridge, UK). All other chemicals used in this study were of analytical grade.

### 2.2 Cell culture and differentiation

3T3-L1 and HIB1B pre-adipocytes (ATCC, Manassas, VA, USA) were cultured in Dulbecco's Modified Eagle's Medium (DMEM, Thermo Fisher Scientific, Waltham, MA, USA) supplemented with 10% fetal bovine serum (FBS, Thermo) and 100 $\mu$g/ml of penicillin-streptomycin (Thermo) at 37℃ in a 5% $CO_2$ incubator. Sufficiently confluent cells were maintained in differentiation induction medium consisting of 10 $\mu$g/ml of insulin (Sigma, St. Louis, MO, USA), 0.25 $\mu$M dexamethasone (Dex, Sigma), and 0.5 mM 3-isobutyl-1-methylxanthine (IBMX, Sigma) in DMEM followed by culturing in maturation medium containing 10% FBS and 10 $\mu$g/ml of insulin. During treatments, unless otherwise stated, cells were maintained in complete medium containing 200 $\mu$M *t*CA (dissolved in dilute ethanol) for 6-8 days before further analysis. Maturation medium was changed every two days. Cytotoxicity of *t*CA was evaluated by MTT assay as described previously (Mosmann., 1983).

### 2.3 Quantitative real-time RT-PCR

Total RNA was isolated from mature cells (4-8 days) using a total RNA isolation kit (RNA-spin, iNtRONBiotechnology, Seongnam, Korea). RNA (1 μg) was converted to cDNA using Maxime RT premix (iNtRON Biotechnology). Power SYBR green (Roche Diagnostics Gmbh, Mannheim, Germany) was employed to quantitatively determine transcription levels of genes by quantitative RT-PCR (Stratagene 246 mix 3000p QPCR System, Agilent Technologies, Santa Clara, CA, USA). PCR reactions were run in duplicates for each sample. Transcription levels of all genes were normalized to the level of β-actin. Sequences of primer sets used in this study are listed in Table 3.

### 2.4 Oil Red O staining

Cells were matured for 4-8 days followed by washing with phosphate-buffered saline (PBS), fixation with 10% formalin for 1 h at room temperature, and washing again three times with deionized water. A mixture of Oil Red O solution (0.6% Oil Red O dye in isopropanol) and water at a 6:4 ratio was layered onto cells for 20 min followed by washing four times with deionized water. Images of the stained lipid droplets were visualized using an inverted microscope. Intracellular lipid content was quantified after extracting ORO bound to cells with 100% isopropanol, and absorbance at 500nm was determined in triplicate wells using a microplate reader.

### 2.5 Immunoblot analysis

Cell lysates were prepared using RIPA buffer (Sigma) by homogenization and centrifugation at 13000 ×g for 30 min. Cell extract was diluted in

5X sample buffer (50 mM Tris at pH 6.8, 2% SDS, 10% glycerol, 5% β-mercaptoethanol, and 0.1% bromophenol blue) and heated at 95℃ for 5 min before 8, 10, or 12% SDS-polyacrylamide gel electrophoresis (PAGE). After electrophoresis, samples were transferred onto a poly vinylidene difluoride membrane (PVDF, ATTO Technology, Amherst, NY, USA) and then blocked for 1 h with TBS-T (10 mM Tris-HCl, 150 mM NaCl, and 0.1% Tween 20) containing 5% skim milk (Sigma) or BSA (Rocky Mountain Biologicals, Missoula, MT, USA). The membrane was rinsed three times consecutively with TBS-T buffer followed by incubation at room temperature for 1 h with 1:1,000 diluted primary polyclonal antibodies, including anti-ATGL, anti-ACC, anti-pACC, anti-β-actin, anti-PPARɣ, anti-AMPK, anti-pAMPK, anti-UCP1, anti-PGC-1α, anti-CPT1, anti-ACOX1, anti-C/EBPα, anti-β3-AR, anti-PKA, anti-FAS (Santa Cruz Biotechnology), anti-PRDM16(Abcam, Cambridge, UK) and anti-pHSL (CST, Massachusettes, USA), in TBS-T buffer containing 1% skim milk or BSA. After three washes, the membrane was incubated with horseradish peroxidase-conjugated anti-goat IgG, anti-rabbit IgG or anti-mouse IgG secondary antibody (1:1000, Santa Cruz Biotechnology) in TBS-T buffer containing 1% skim milk or BSA at room temperature for 1 h. Immunoblots were then developed with enhanced chemiluminescence and captured with ImageQuant LAS500 (GE, Malborough, MA, USA). Every experiment was representative of three independent experiments. Protein band intensities were normalized using β-actin bands in each cell sample and band intensities were quantified ImageJ software (NIH, Bethesda, MD, USA).

### 2.6 Immunocytochemistry

Immunocytochemistry was performed on formalin-fixed cells. These cells were incubated with anti-UCP1 (dilution 1:1000, Santa Cruz Biotechno

logy) primary antibody at 4ºC overnight followed by incubation with appro priate FITC goat anti-mouse secondary antibody at room temperature for 4 h. For staining of mitochondria, MitoTracker®Red(1mM,CellSignalingTechnol ogy)wasdirectlyaddedtoPBB-T(PBS+1%BSAand0.1%Tween20)ataconcentratio nof200nM.Cellswerethenincubatedat37ºCfor2h.Afterincubation,tissueswerewash edwithPBSandsubjectedtoimmunostaining.Morphologicalfindingswereobserved usingalightmicroscopeatX40magnification.

### 2.7 Statistical analysis

All data are presented as mean ± SD of at least three independent experiments. Statistical significance among multiple groups was determined by one-way analysis of variance (ANOVA) followed by Tukey's post-hoc test or two-tailed Student's *t*-test using Statistical Package of Social Scien ce (SPSS) software version 17.0 (SPSS Inc., Chicago, IL, USA). Statistical significance was indicated as either $p < 0.05$ or $p < 0.01$.

# 3. Results

## 3.1 *Trans*-cinnamic acid (*t*CA) induces browning in 3T3-L1 white adipocytes

First, *t*CA cytotoxicity to 3T3-L1 preadipocytes was evaluated by MTT assay. As shown in Fig. 8B, *t*CA resulted in no significant cytotoxicity at concentration up to 400 μM. Hence, unless otherwise stated, cells were treated with 200 μM *t*CA to investigate its browning effect. As shown in Fig. 8C, *t*CA significantly upregulated the expression of brown-fat - specific proteins UCP1, PRDM16, and PGC-1α in a dose-dependent manner. It also significantly upregulated genes *Ppargc1a, Prdm16* and *Ucp1* and beige-fat -specific genes *Cd137*, *Cited1*, *Tbx1*, and *Trem26* (Fig. 8D).

## 3.2 *t*CA activates HIB1B brown adipocytes

Since *t*CA showed no detectable cytotoxicity at concentration up to 400 μM (Fig. 9A), we further investigated whether *t*CA could activate HIB1B brown adipocytes. To this end, we allowed HIB1B adipocytes to differentiate in complete media containing different concentrations of *t*CA (0-200 μM). Our results demonstrated that *t*CA strikingly activated HIB1B brown adipocytes by enhancing expression levels of brown fat-specific proteins UCP1, PRDM16, and PGC-1α in a dose-dependent manner (Fig. 9B). It also significantly upregulated brown-fat signature genes *Cidea*, *Lhx8*, *Ppargc1a*, *Prdm16*, *Ucp1*, and *Zic1* at concentration of 50 μM (Fig. 9C). Next, we determined expression levels of key adipogenic transcription factors (C/EBPα and PPARγ) in HIB1B adipocytes. Their expression levels were remarkably elevated upon *t*CA treatment (50 μM) (Fig. 9D), suggesting that *t*CA could

stimulate adipogenesis in brown adipocytes. In addition, *t*CA treatment (50 μM) decreased intensity of Oil Red O staining (Fig. 9E).

### 3.3 *t*CA activates thermogenesis in white and brown adipocytes

As mentioned previously, *t*CA activated thermogenic marker proteins in both white and brown adipocytes. To confirm this result at genetic level we verified the mitochondrial biogenic genes *Cox4, Nrf1, MtDNA* and *Tfam* which expressed an elevated expression as well as at cellular level, where we directly detected UCP1 protein levels in both differentiated adipocytes using immunofluorescent staining with MitoTracker®Red.Resultsrevealedstrongersignalsin *t*CA-treated 3T3-L1 (Fig. 10A) and HIB1B (Fig. 10B) adipocytes compared to those in both control adipocytes.

### 3.4 *t*CA regulates lipid metabolism in white adipocytes

Next, we investigated the effect of *t*CA on lipid metabolism in white adipocytes. For this, we determined expression levels of key adipogenic transcription factors such as C/EBPα and PPARγ in 3T3-L1 white adipocytes. Different from results shown in brown adipocytes, their expression levels were reduced upon *t*CA treatment, suggesting decreased adipogenesis (Fig. 11A). Recruitment of beige cells in 3T3-L1 adipocytes consequently led to reduced fat accumulation as evidenced by reduced triglycerides after *t*CA treatment (Fig. 11B). Moreover, expression levels of acetyl-CoA carboxylase (ACC) and fatty acid synthase (FAS) as important lipogenic markers were markedly reduced upon *t*CA treatment along with an increased ratio of pACC to total ACC mediated by AMPK activation (Fig. 11C). Next, we inves

tigated expression levels of lipolysis-related proteins including phosphorylated (activated) hormone-sensitive lipase (pHSL) and adipocyte triglyceride lipase (ATGL) before and after *t*CA treatment. As shown in Fig. 11D, *t*CA enhanced lipolysis by increasing expression levels of pHSL and ATGL. *t*CA treatment also significantly increased mitochondrial protein levels of acyl-coenzyme A oxidase 1 (ACOX1) and carnitine palmitoyl transferase 1 (CPT1), suggesting augmented oxidative capacity upon *t*CA treatment (Fig. 11E).

### 3.5 *t*CA induces browning of white adipocytes via activation of β3-AR and AMPK signaling pathway

We further investigated molecular mechanisms involved in the browning activity of *t*CA. To this end, we separately treated cells with β3-adrenergic receptor (β3-AR) antagonist L-748.337 at 80 μM and β3-AR agonist BRL 37344 at 20 μM with or without *t*CA at 200 μM after 7 days of differentiation, after which expression levels of key signaling molecules (PGC-1α, PRDM16, and UCP1) responsible for browning were determined. Inhibition of β3-AR by antagonist L-748,337 resulted in reduced expression levels of PKA, pAMPK, and browning markers. It also abolished increment of β3-AR, PKA, pAMPK, and browning markers induced by *t*CA (Fig. 12A). Treatment with β3-AR agonist BRL 37344 in combination with *t*CA synergistically increased expression levels of β3-AR, PKA, pAMPK, and browning marker proteins (Fig. 12A). We also determined expression levels of browning marker proteins PRDM16, PGC-1α, and UCP1 after separate treatment of 3T3-L1 cells with AMPK antagonist dorsomorphin at 5 μM and AMPK agonist AICAR at 100 μM after 7 days of differentiation. Inhibited AMPK decreased expression levels of browning markers and abolished their increased levels induced by *t*CA. Browning markers were also synergistically ele

vated by a combination of AMPK agonist and *t*CA (Fig. 12B). In addition, *tCA* elevated the expression levels upto two-fold for ATGL and p-HSL in the presence of β3-AR agonist, indicating its potential role of lipolysis med iated by β3-AR in white adipocytes (Supp. Fig. 7). These results indicate that AMPK has a direct effect on browning and elevated thermogenesis in duced by *t*CA through β3-AR signaling pathway in 3T3-L1 white adipocyt es (Fig. 13).

Table 3. List of primers used for real-time quantitative RT-PCR

| Gene | Accession no. | Forward | Reverse |
|---|---|---|---|
| *Cd137* | DQ832278.1 | GGTCTGTGCTTAAGACCGGG | TCTTAATAGCTGGTCCTCCCTC |
| *Cidea* | NM_007702.2 | CGGGAATAGCCAGAGTCACC | TGTGCATCGGATGTCGTAGG |
| *Cited1* | NM_001276466.1 | GGAAGGCACAGCACCCACTC | GGAAGGCACAGCACCCACTC |
| *Cox4* | NM_001293559.1 | TGACGGCCTTGGACGG | CGATCAGCGTAAGTGGGGA |
| *Lhx8* | NM_010713.2 | CATCGCTGTTCTGCCTGTTAG | CTCGGGATTCAGCAGTCCTTC |
| *Nrf1* | NM_010938.4 | GCTAATGGCCTGGTCCAGAT | CTGCGCTGTCCGATATCCTG |
| *Ppargc1a* | NM_008904.2 | ATGAATGCAGCGGTCTTAGC | AACAATGGCAGGGTTTGTTC |
| *Prdm16* | NM_027504.3 | GATGGGAGATGCTGACGGAT | TGATCTGACACATGGCGAGG |
| *Tbx1* | NM_001285472.1 | AGCGAGGCGGAAGGGA | CCTGGTGACTGTGCTGAAGT |
| *Tfam* | BC083084.1 | ATGTGGAGCGTGCTAAAAGC | GGATAGCTACCCATGCTGCTGGAA |
| *Tmem26* | NM_177794.3 | CCATGGAAACCAGTATTGCAGC | ATTGGTGGCTCTGTGGGATG |
| *Ucp1* | NM_009463.3 | CCTGCCTCTCTCGGAAACAA | GTAGCGGGGTTTGATCCCAT |
| *Zic1* | NM_009573.3 | GCCACAAATCCGGGAAGAAG | CTCACTTTCTCGCCGCTCAG |

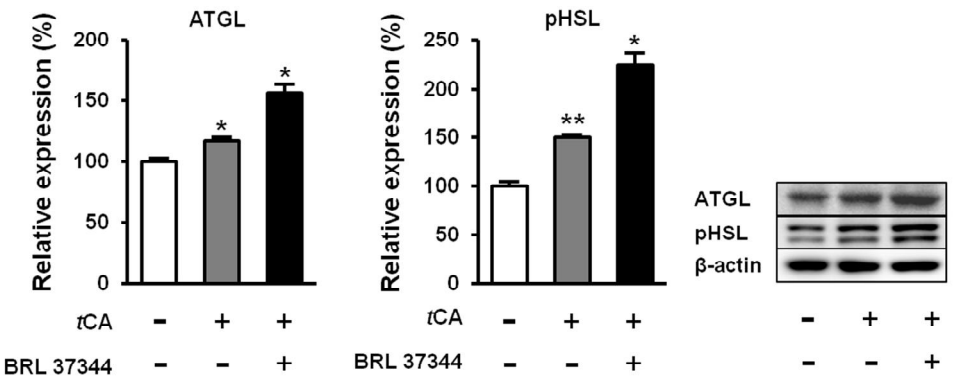


Supplementary Fig. 7. *Trans*-cinnamic acid (*t*CA) elevated the expression levels upto two-fold for ATGL and p-HSL.

Activation of β3-AR by its agonist (BRL 37344) resulted in increased expression of ATGL and pHSL lipolysis markers. Data are presented as mean ± S.D.. Differences between groups were determined by one-way analysis of variance (ANOVA) followed by Tukey's post-hoc test or two-tailed Student's *t*-test using Statistical Package of Social Science (SPSS) software version 17.0 (SPSS Inc., Chicago, IL, USA). Statistical significance between control and *t*CA-treated 3T3-L1 cells is shown as $^{*}p < 0.05$ or $^{**}p < 0.01$.

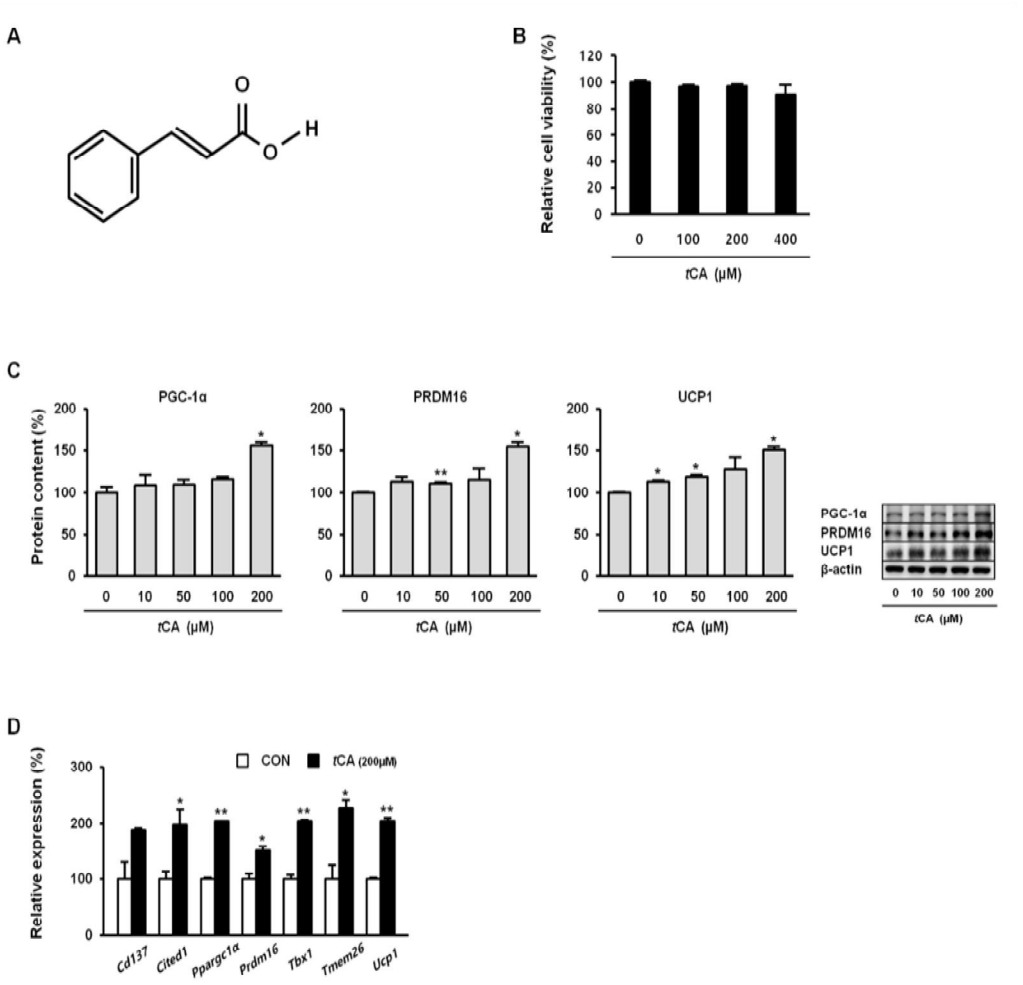


Fig. 8. *Trans*-cinnamic acid (tCA) induces fat browning in 3T3-L1 white adipocytes. Chemical structure of *t*CA(A) and cytotoxicity of *t*CA (B). *t*CA at 200 μM promotes increased expression of core brown fat marker proteins (C) in a dose-dependent manner as well as beige fat-specific genes (D) in 3T3-L1 adipocytes. Data are presented as mean ± S.D.. Differences between groups were determined by one-way analysis of variance (ANOVA) followed by Tukey's post-hoc test or two-tailed Student's *t*-test using Statistical Package of Social Science (SPSS) software version 17.0 (SPSS Inc., Chicago, IL, USA). Statistical significance between control and *t*CA-treated 3T3-L1 cells is shown as $^{*}p < 0.05$ or $^{**}p < 0.01$.

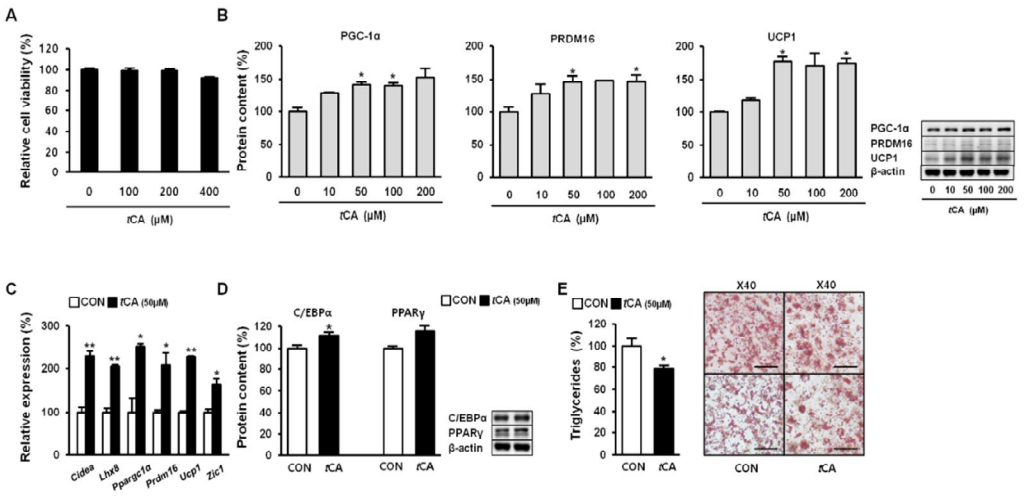


Fig. 9. *Trans*-cinnamic acid (*t*CA) activates brown adipocytes.

Cytotoxicity of *t*CA in HIB1B cells (A). *t*CA (50 μM) elevates expression levels of core brown fat marker proteins (B) in a dose-dependent manner as well as brown fat-specific genes (C) in HIB1B adipocytes and increases adipogenesis (D). Repres entative images of Oil Red O staining of HIB1B cells taken at X40 magnification (scale bar = 50 μm). Lipid content was quantified by extracting Oil Red O stain b ound to cells with 100% isopropanol in brown adipocytes (E). Data are presented a s mean ± S.D.. Differences between groups were determined by one-way analysis of variance (ANOVA) followed by Tukey's post-hoc test or two-tailed Student's *t* -test using Statistical Package of Social Science (SPSS) software version 17.0 (SP SS Inc., Chicago, IL, USA). Statistical significance between control and *t*CA-treate d HIB1B cells is shown as $^{*}p < 0.05$ or $^{**}p < 0.01$.

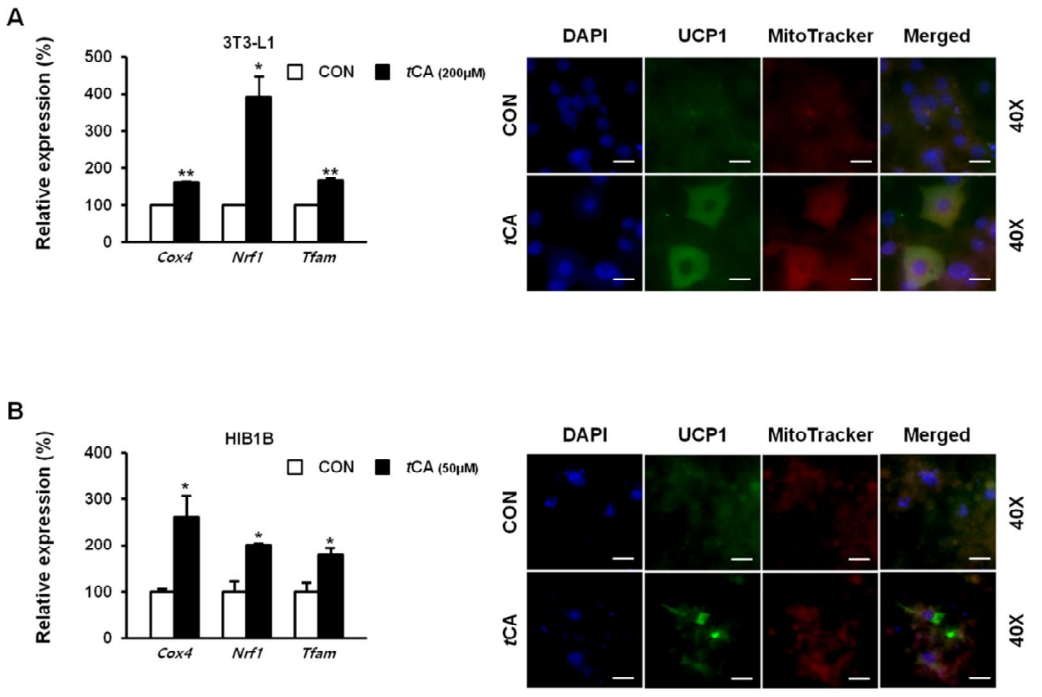


Fig. 10. Activation of UCP1 by *trans*-cinnamic acid (*t*CA).

Immunocytochemistry staining of differentiated 3T3-L1 white adipocytes (scale bar s=50 μm) (A) and HIB1B brown adipocytes (scale bar = 20 μm) (B) with MitoTracker Red dye used for UCP1 detection after treatment with 50 μM of *t*CA. Images were captured at 40X magnification.

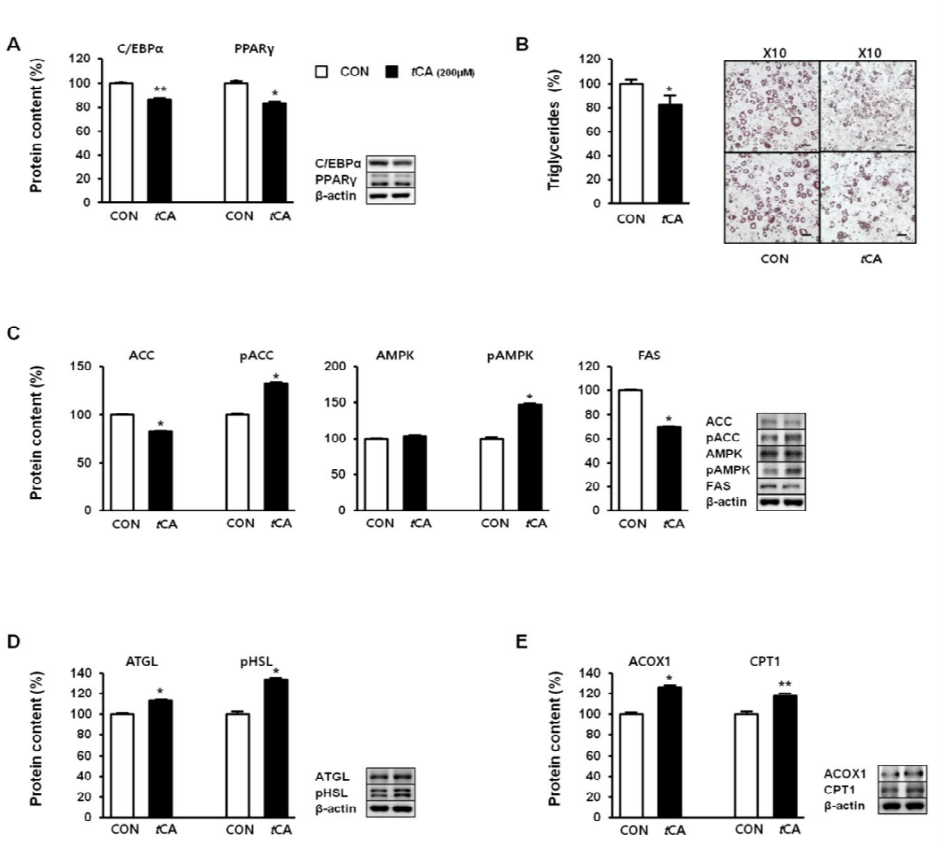


Fig. 11. *Trans*-cinnamic acid (*t*CA) regulates lipid metabolism in white adipocytes. *t*CA decreases adipogenesis by down-regulating key adipogenic transcription factors (A). Representative images of Oil Red O staining of 3T3-L1 were taken at X 10 magnification (scale bar = 100 μm). Lipid content was quantified by extracting Oil Red O stain bound to cells with 100% isopropanol in 3T3-L1 adipocytes (B). tCA regulates lipogenic (C), lipolytic (D), and fatty acid oxidative markers (E). Data are presented as mean ±S.D.. Differences between groups were determined using Student's *t*-test. Statistical significance between control and *t*CA-treated 3T3-L1 cells is shown as $*p < 0.05$ or $**p < 0.01$.

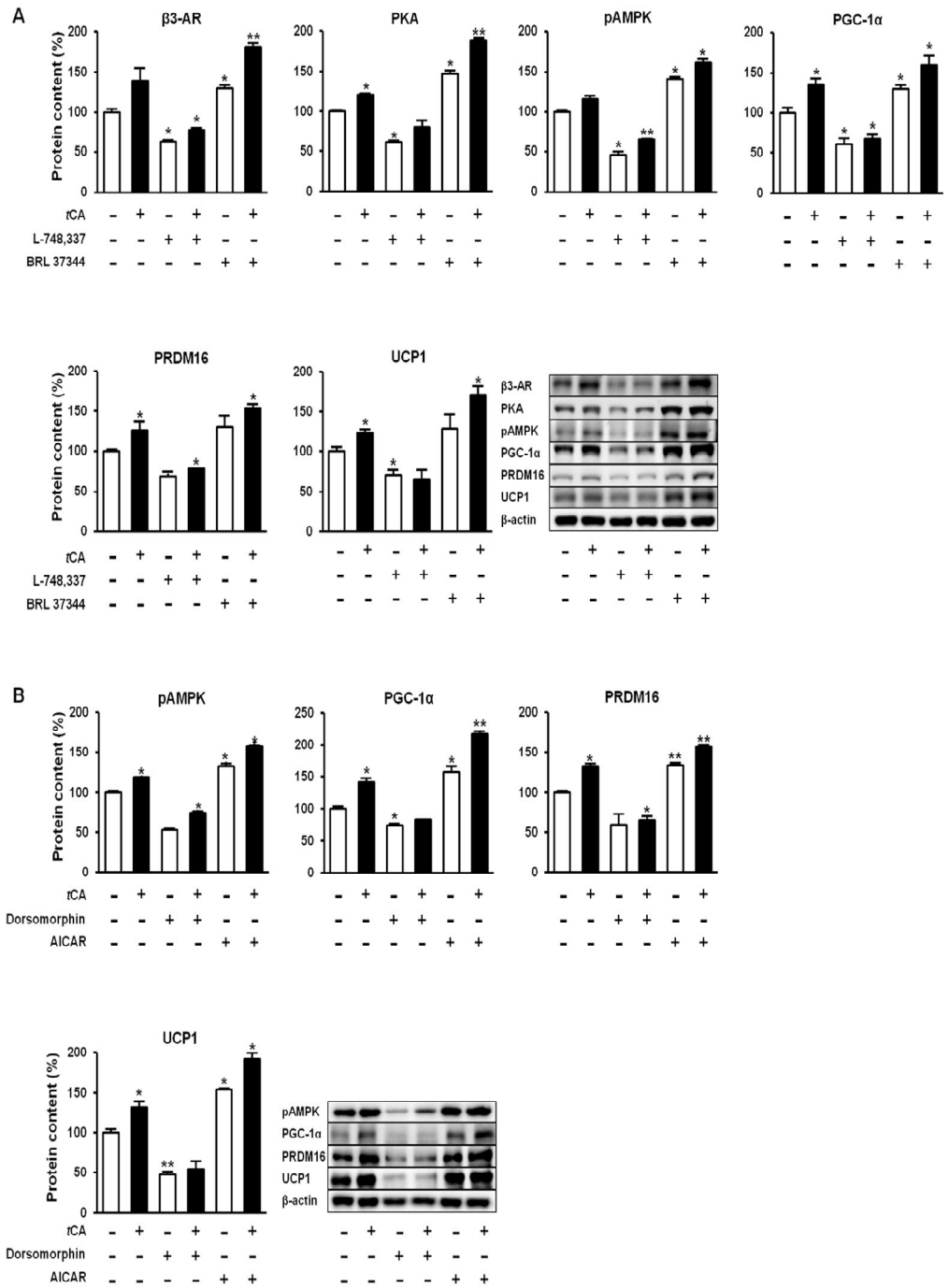
A
β3-AR
PKA
pAMPK
PGC-1α
PRDM16
UCP1
Protein content (%)
tCA
L-748,337
BRL 37344
β-actin
B
pAMPK
PGC-1α
PRDM16
UCP1
Dorsomorphin
AICAR

Fig. 12. *Trans*-cinnamic acid (*t*CA) induces browning of white adipocytes via activation of β3-AR and AMPK signaling pathway.

Inhibition of β3-AR by its antagonist (L-748.337) resulted in decreased expression of PKA, pAMPK, PRDM16, PGC-1α, and UCP1 (A). Similarly, suppression of AMPK by antagonist (dorsomorphin) caused reduced expression of UCP1, pAMPK, PRDM16, and PGC1-α whereas agonist (AICAR) resulted in increased expression of browning markers (B). Data are presented as mean ± S.D.. Differences between groups were determined by one-way analysis of variance (ANOVA) followed by Tukey's post-hoc test or two-tailed Student's *t*-test using Statistical Package of Social Science (SPSS) software version 17.0 (SPSS Inc., Chicago, IL, USA). Statistical significance between control and *t*CA-treated 3T3-L1 cells is shown as $*p < 0.05$ or $**p < 0.01$.

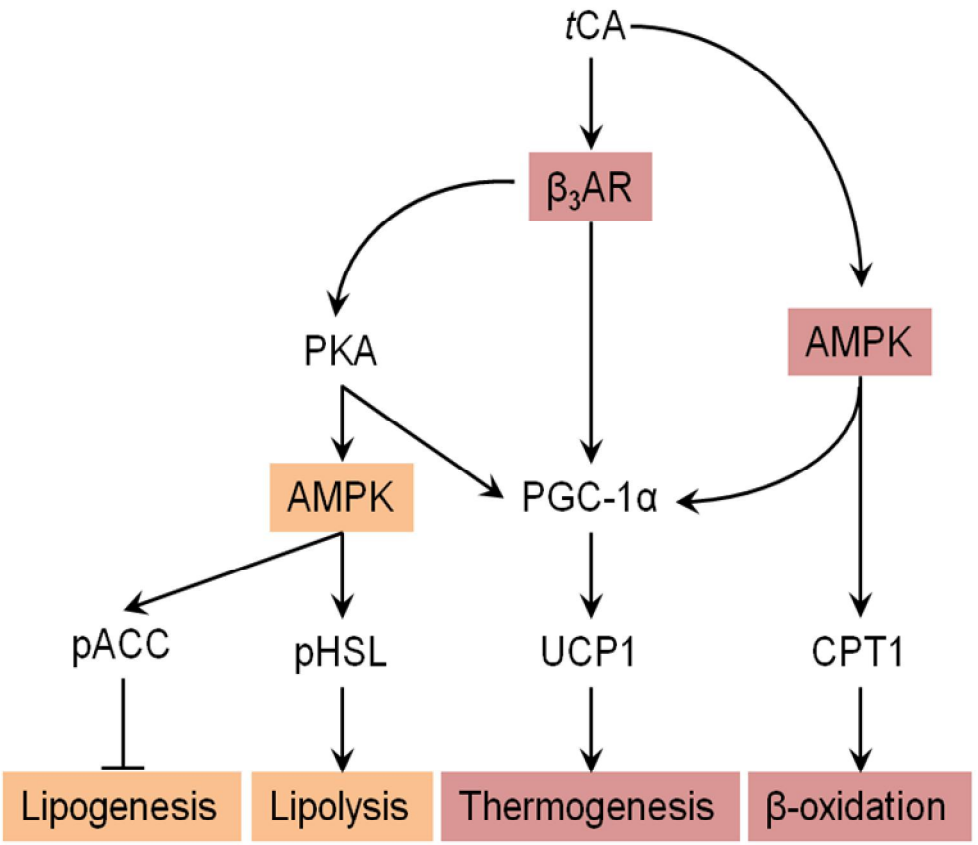


Fig. 13. Suggested pathway for *t*CA -induced browning via β3-AR and AMPK signaling pathway.

Arrow indicates stimulated regulation by *t*CA and T refers to supressed regulation by *t*CA.

# 4. Discussion

Results of the present study showed that *t*CA treatment could activ ate thermogenic and metabolic responses in 3T3-L1 white adipocytes, with a focus on the induction of beige adipocytes and elucidated the underlying molecular mechanism. Over many years, cinnamon and its derivatives have been used in traditional medicine to treat diabetes, obesity, and other meta bolic diseases (Kopp et al., 2014; Qin et al., 2010; Adisakwattana et al., 201 7). *t*CA is one of the active components of cinnamon, a spice produced fro m the bark of *Cinnamomum*. Numerous health benefits have been ascribed to cinnamon and cinnamon extract has been commercially sold to treat dia betes and other metabolic syndromes (Rafehi et al., 2012). Despite a lot of reports about the beneficial roles of cinnamon and its derivatives in obesit y, there is neither a consensus about bioactive constituents of cinnamon dri ving these effects nor molecular pathways responsible for its benefits (Rafe hi et al., 2012; Verspohl et al., 2005; Camacho et al., 2015). Results obtaine d here contribute to the clarification of the active component in cinnamon a nd potential pathways involved in browning and other metabolic responses.

Recently, Kwan et al. (2017) have reported that cinnamon extract ha s browning effect in subcutaneous adipocytes of *db/db* and diet-induced ob ese mice via β3-AR signaling (Kwan et al., 2015). They have identified th at components in cinnamon extract are protocatechuic acid, catechin, chloro genic acid, and sesculetin. However, they did not specify which component was mainly involved in browning. Our data support that *t*CA might play a n important role in the browning effect of cinnamon extract, although effec ts of other cinnamon components such as cinnamadehyde and cinnamate sh ould be determined in the future. *t*CA-mediated browning also follows β-a drenergic signaling pathway through consequent activation of PKA and A

MPK. However, possibility for TRPA1-agonistic action of *t*CA in browning effect cannot be excluded as cinnamaldehyde, one of the active components and 90% of the essential oil of cinnamon bark, can activate TRPA1 and in crease thermogenesis (Camacho et al., 2015; Tamura et al., 2012). Thermog enic activity of cinnamaldehyde needs to be determined as it is easily oxidi zed to cinnamic acid. Cinnamaldehyde, an essential oil found in cinnamon, i s also protective against obesity in mouse models by activating thermogen esis through PKA-p38 MAPK signaling pathway (Camacho et al., 2015; Jia ng et al., 2018). Taken together, it is likely that cinnamon and its derivativ es have thermogenic activity in adipocytes via TRPA1 and/or β3AR-PKA signaling pathway.

In adipogenesis, two transcription factors such as C/EBPα and PPA Rɣ tightly regulate the development of preadipocytes into mature adipocyte s (Rosen et al., 2002). Suppressing these factors will reduce the accumulati on of TG (Farmer et al., 2006). Hsu et al. (2007) have reported that *o*-hyd roxycinnamic acid can inhibit adipogenesis in 3T3-L1 adipocytes by inhibiti ng glycerol-3-phosphate dehydrogenase activity and down-regulating adipo genic transcription factors (Hsu et al., 2007). Similarly, *p*-hydroxycinnamic acid can suppresses adipogenesis in 3T3-L1 preadipocytes by inhibiting M APK/ERK signaling pathway (Yamaguchi et al., 2013). Identical results are found with Esculetin derived from coumarin, which displayed reduced adipo genesis modulated by the AMPK pathway in 3T3-L1 adipocytes (Wang et al., 2015).

One of the important targets of AMPK is acetyl-CoA carboxylase (ACC), a key enzyme of lipogenesis by converting acetyl-CoA to malonyl-CoA. When ACC is phosphorylated (activated), action of ACC is inhibited, thereby suppressing lipogenesis (Daval et al., 2006). Phosphorylation of AM PK and ACC by *t*CA is related to increased mitochondrial fatty acid oxidat

ion in adipocytes (Fang et al., 2018). This finding is supported by increased expression of ACOX and CPT1, key players of fatty acid oxidation, upon *t*CA treatment. Work by Prabhakar and Doble (2011) and our current data support that *t*CA can reduce the expression of fatty acid synthase, thereby alleviating TG accumulation in adipocytes (Prabhakar et al., 2014), moreover our experiments also suggested that *tCA* could decrease lipid accumulation in white adipocytes. Recent studies have demonstrated that lipogenesis and lipolysis are coupled in adipose tissue during chronic β3-AR stimulation (Mottillo et al., 2014). Enhanced lipid catabolism by *t*CA is likely to be responsible for major metabolic adaptations during conversion of white to beige adipocytes (Barquissau et al., 2016). Collectively, *t*CA and its derivatives could be effective compounds for improving adipocyte function.

It is well recognized that activated AMPK can switch on catabolic pathways such as glycolysis and fatty acid oxidation and inhibit anabolic processes such as lipogenesis in white adipocytes (Daval et al., 2006). Despite its importance in energy homeostasis, the role of AMPK in adipocyte lipolysis remains controversial. Yin and Birnbaum (2003) have demonstrated that AMPK activation is required for maximal increase in lipolysis induced by β-adrenergic stimulation (Yin et al., 2003). In contrast, Daval et al. (2005) have argued that AMPK can block translocation of HSL to lipid droplets, thereby inhibiting lipolysis (Daval et al., 2005). Our indirect evidence suggested that *t*CA-mediated AMPK activation could lead to stimulated lipolysis by increasing expression levels of ATGL and pHSL. The β-adrenergic signaling pathway represents a prime regulator of triglyceride breakdown by PKA-dependent phosphorylation of HSL. In the current study, *t*CA obviously activated β3-AR and consequently activated PKA, thereby phosphorylating HSL. An alternative way to activate AMPK in 3T3-L1 adipocytes has been reported by Kopp et al. (2014), demonstrating that *t*CA can activate AMPK by G-protein-coupled receptor (GPR) signaling (Kopp et al., 2014).

Cold-mediated browning works practically only on beige fat depots whereas classical brown adipocytes would be physiologically uninteresting for the browning process as only a modest increase in UCP1 level has been detected as an effect of cold (Kalinovich et al., 2017). In contrast, many browning agents can induce white fat browning and activate classical brown adipocytes (Lone et al., 2016; Parray et al.,2016; Choi et al., 2018). From this point of view, searching for agents such as *t*CA that can activate both white fat browning and brown fat would be a promising therapeutic strategy against obesity.

In summary, anti-obesity effect of *t*CA was due to suppressed adipogenesis and lipogenesis as well as increased fat oxidation and enhanced thermogenesis in adipocytes where β3AR-PKA-AMPK, TRPA1, GPR signaling pathways were responsible for thermogenic activity of *t*CA and its related components. Considering long half-life of compounds in cinnamon (Zhao et al., 2014) and good bioavailability (El-Seedi et al., 2012), consumption of *t*CA by oral administration may be a feasible way to activate thermogenesis and improve systematic lipid metabolism, thus ultimately protecting against obesity and other metabolic disorders in humans.

# REFERENCES


Adisakwattana, S. Cinnamic acid and its derivatives: mechanisms for prevention and management of diabetes and its complications. Nutrients 2017, 9, 163.

Anderson, R.A., Broadhurst, C.L., Polansky, M.M., Schmidt, W.F., Khan, A., Flanag an, V.P., Scgoene, N.W., Graves, D.F. Isolation and characterization of polyp henol type-A polymers from cinnamon with insulin-like biological activity. J. Agric. Food. Chem. 2014, 52, 65-70.

Aprotosoaie, A. C., Costache, II., Miron, A., Anethole and Its Role in Chronic Diseases. Adv Exp Med Biol 2016, 929, 247-267.

Azhar, Y., Parmar, A., Miller, C. N., Samuels, J. S., Rayalam, S., Phytochemicals as novel agents for the induction of browning in white adipose tissue. Nutr. Metab. 2016, 13, 39.

Azhar, Y., Parmar, A., Miller, C.N., Samuels, J.S., Rayalam, S. Phytochemicals as novel agents for the induction of browning in white adipose tissue. Nutr. M etab (Lond). 2016, 13, 89.

Azzu, V., Brand, M.D. The on-off switches of the mitochondrial uncoupling protein s. Trends. Biochem. Sci. 2010, 35, 298-307.

Bae, J. P., Lage, M. J., Mo, D., Nelson, D. R., Hoogwerf, B. J., Obesity and glyce mic control in patients with diabetes mellitus: Analysis of physician electron ic health records in the US from 2009-2011. J. Diabetes Complications 2015, 30, 212-20.

Barceloux, D.G. Cinnamon (Cinnamomum species) Medical toxicology of natural su bstances. John Wiley & Sons 2009, 327-335.

Barquissau, V., Beuzelin, D., Pisani, D.F., Beranger, G.E., Mairal, A., Montagner, A., Roussel, B., Tavrnier, G., Marques, M.A., Moro, C. et al. White-to-brite conversion in human adipocytes promotes metabolic reprogramming towards fatty acid anabolic and catabolic pathways. Mol. Metab. 2016, 5, 352-365.

Barquissau, V., Beuzelin, D., Pisani, D.F., Beranger, G.E., Mairal, A.; Montagner, A., Roussel, B., Tavernier, G., Marques M.A., Moro, C., et al. White-to-brit e conversion in human adipocytes promotes metabolic reprogramming towar

ds fatty acid anabolic and catabolic pathways. Mol. Metab. 2016, 5, 352-365.

Bartonkova, I., Dvorak, Z., Essential oils of culinary herbs and spices display agoni st and antagonist activities at human aryl hydrocarbon receptor AhR. Food Chem. Toxicol. 2017, 111, 374-384.

Bhattacharjee, R., Devi, A., Mishra, S., Molecular docking and molecular dynamics studies reveal structural basis of inhibition and selectivity of inhibitors EGC G and OSU-03012 toward glucose reglated protein-78 (GRP78) overexpresse d in glioblastoma. J. Mol. Model. 2015, 21, 272.

Bonet, M.L., Oliver, P., Palou, A. Pharmacological and nutritional agents promoting browning of white adipose tissue. Biochim. Biophys. Acta. 2018, 1831, 969-9 85.

Bonet, S. D., Dixit, V. D., Kahn, C. R., Leibel, R. L., Lin, X., Nieuwdrop, M., Pietil ainen, K. H., Rabasa-Lhoret, R., Roden, M., Scherer, P. E., Klein, S., Metab olically healthy and unhealthy obese—the 2013 Stock Conference report. Obe se. Rev. 2014, 15, 697-708.

Boutant, M., Joffraud, M., Kulkarni, S. S., Garcia-Casarrubios, E., Garcia-Roves, P. M., Ratajczak, J., Fernandez-Marcos, P. J., Valverde, A. M., Serrano, M., Ca nto, C., SIRT1 enhances glucose tolerance by potentiating brown adipose tis sue function. Mol. Metab. 2015, 4, 118-131.

Calderon-Dominguez, M., Mir, J. F., Fucho, R., Weber, M., Serra, D., Herrero, L., Fatty acid metabolism and the basis of brown adipose tissue function. Adip ocyte 2016, 5, 98-118.

Camacho, S., Michlig, S., de Senarclens-Bezençon, C., Meylan, J., Meystre, J., Pezz oli, M., Markram, H., le Coutre, J. Anti-obesity and anti-hyperglycemic effe cts of cinnamaldehyde via altered ghrelin secretion and functional impact on food intake and gastric emptying. Sci. Rep. 2015, 5, 7919.

Carey, A.L., Vorlander, C., Reddy-Luthmoodoo, M., Natoli, A.K., Formosa, M.F., Be rtovic, D.A., Anderson, M.J., Duffy, S.J., Kingwell B.A. Reduced UCP-1 cont ent in in vitro differentiated beige/brite adipocytes derived from preadipocyte s of human subcutaneous white adipose tissues in obesity. PLoS One 2014, 9, e 91997.

Cavalcanti, J. M., Leal-Cardoso, J. H., Diniz, L. R., Portella, V. G., Costa, C. O., Li

nard, C. F., Alves, K., Rocha, M. V., Lima, C. C., Cecatto, V. M., Coelho-de-Seouza, A. N., The Essential Oil of Croton Zehntneri and Trans-Anethole Improves Cutaneous Wound Healing. J. Ethnopharmacol. 2012, 144, 240-7.

Chen, A. Y., Kim, S. E., Prevalence of Obesity Among Children With Chronic Conditions. Obesity 2009, 18, 210-3.

Chen, C. H., deGraffenried, L. A., Anethole Suppressed Cell Survival and Induced Apoptosis in Human Breast Cancer Cells Independent of Estrogen Receptor Status. Phytomedicine 2012, 19, 763-7.

Choi, K. M., Sarcopenia and sarcopenic obesity. Korean J. Intern. Med. 2016, 31, 1054-1060.

Choi, M.J., Mukherjee, S., Kang, N.H., Barkat, J.L., Parray, H.A., Yun, J.W. LRhamnose induces browning in 3T3L1 white adipocytes and activates HIB1B brown adipocytes. IUBMB Life 2018, 70, 563-573.

Choi, Y., Lee, Y. H., Park, S. K., Cho, H., Ahn, K. J., Association between obesity and local control of advanced rectal cancer after combined surgery and radiotherapy. Radiat. Oncol. J. 2016, 34, 113-120.

Claussnitzer, M., Dankel, S.N., Kim, K.H., Quon, G., Meuleman, W., Haugen, C., Glunk, V., Sousa, I.S., Beaudry J.L., Puviindran, V., et al. FTO Obesity Variant Circuitry and Adipocyte Browning in Humans. N. Engl. J. Med. 2015, 373, 895-907.

Collins, S., β-Adrenoceptor Signalling Networks in Adipocytes for Recruiting Stored Fat and Energy Expenditure. Front Endocrinol(Lausanne) 2011, 2, 102.

Daval, M., Diot-Dupuy, F., Bazin, R., Hainault, I., Viollet, B., Vaulont, S., Hajduch, E., Ferré, P., Foufelle, F. Anti-lipolytic action of AMP-activated protein kinase in rodent adipocytes. J. Biol. Chem. 2005, 280, 25250-25257.

Daval, M., Foufelle, F., Ferré, P. Functions of AMP-activated protein kinase in adipose tissue. J. Physiol. 2006, 574, 55 - 62.

Dongare, V., Kulkarni, C., Kondawar, M., Magdum, C., Haldavnekar, V., Arvindekar, A., Inhibition of aldose reductase and anti-cataract action of trans-anethole isolated from Foeniculum vulgarae Mill. Fruits. Food chem. 2012, 132, 385-90.

El-Seedi, H.R., El-Said, A.M., Khalifa, S.A., Göransson, U., Bohlin, L., Borg-Karlso

n, A.K., Verpoorte, R. Biosynthesis, natural sources, dietary intake, pharmac okinetic properties, and biological activities of hydroxycinnamic acids. J. Agr ic. Food Chem. 2012, 60, 10877-10895.

Fang, C., Kim, H., Noratto, G., Sun, Y., Talcott, S.T., Mertens-Talcott, S.U. Gallot annin derivatives from mango (Mangifera indica L.) suppress adipogenesis a nd increase thermogenesis in 3T3-L1 adipocytes in part through the AMPK pathway. J. Funct. Foods 2018, 46, 101-109.

Farmer, S.R. Transcriptional control of adipocyte formation. Cell. Metab. 2006, 4, 2 63 - 273.

Fisher, F.M., Kleiner, S., Douris, N., Fox, E.C., Mepani, R.J., Verdeguer, F., Wu, J., kharitonenkov, A., Flier, J.S., Maratos-Flier, E., et al. FGF21 regulates PGC -1α and browning of white adipose tissues in adaptive thermogenesis. Gene s 2012, 26, 271-281.

Freire, R. S., Morais, S. M., Catunda-Junior, F. E., Pinheiro, D. C., Synthesis and Antioxidant, Anti-Inflammatory and Gastroprotector Activities of Anethole a nd Related Compounds. Bioorg. Med. Chem. 2005, 13, 4353-8.

Galicka, A., Kretowski, R., Nazaruk, J., Cechowska-Pasko, M., Anethole Prevents Hydrogen Peroxide-Induced Apoptosis and Collagen Metabolism Alterations in Human Skin Fibroblasts. Mol. Cell Biochem. 2014, 394, 217-24.

Gonzalez-Hurtado, E., Lee, J., Choi, J., Wolfgang, M. J., Fatty acid oxidation is req uired for active and quiescent brown adipose tissue maintenance and thermo genic programming. Mol. Metab. 2018, 7, 45-56.

Gorelick, N. J., Genotoxicity of Trans-Anethole in Vitro. Mutat. Res. 1995, 326, 199 -209.

Hall, R. L., Oser, B. L., The safety of flavoring substances. In: Gunther F.A. (eds) 24. Springer, New York, NY 1968.

Harms, M.; Seale, P. Brown and beige fat: development, function and therapeutic p otential. Nat. Med. 2013, 19, 1252-1263.

Hsu, C.L., Yen, G.C. Effects of flavonoids and phenolic acids on the inhibition of a dipogenesis in 3T3-L1 adipocytes. J. Agric. Food Chem. 2007, 55, 8404-8410.

Jain, G.S., Puri, S., Misra, A., Gulati, S., Mani, K. Effect of oral cinnamon interven tion on metabolic profile and body composition of Asian Indians with metab

olic syndrome: a randomized double -blind control trial. Lipids Health Dis. 2017, 16, 113.

Jang, M.H. Kang, N.H.; Mukherjee, S.; Yun, J.W. Theobromine, a methylzanthine in cocoa bean, stimulates thermogenesis by inducing white fat browning and activating brown adipocytes. Biotechnol. Bioprocess Eng. 2018, 23,617-626.

Jiang, L., Tang, Z. Expression and regulation of the ERK1/2 and p38 MAPK signaling pathways in periodontal tissue remodeling of orthodontic tooth movement. Mol. Med. Rep. 2018, 17, 1499-1506.

Kalinovich, A.V., de Jong, J.M., Cannon, B., Nedergaard, J. UCP1 in adipose tissues: two steps to full browning. Biochimie 2017, 134, 127-137.

Kang, N.H., Mukherjee, S., Min, T., Kang, S.C., Yun, J.W. Trans-anethole ameliorates obesity via induction of browning in white adipocytes and activation of brown adipocytes. Biochimie 2018, 151, 1-13.

Kang, P., Kim, K. Y., Lee, H. S., Min, S. S., Seol, G. H., Anti-Inflammatory Effects of Anethole in Lipopolysaccharide-Induced Acute Lung Injury in Mice. Life Sci. 2013, 93, 955-61.

Kopp, C., Singh, S.P., Regenhard, P., Müller, U., Sauerwein, H., Mielenz, M. Trans-cinnamic acid increases adiponectin and the phosphorylation of AMP-activated protein kinase through G-protein-coupled receptor signaling in 3T3-L1 adipocytes. Int. J. Mol. Sci. 2014, 15, 2906-2915.

Kwan, H.Y., Wu, J., Su, T., Chao, X.J., Liu, B., Fu, X., Chan C.L., Lau, R.H.Y., Tse, A.K.W., Han, Q.B., et al. Cinnamon induces browning in subcutaneous adipocytes. Sci. Rep. 2015, 7, 2447.

Lee, M. H., Chen, Y. Y., Tsai, J. W., Wang, S. C., Watanabe, T., Tsai, Y. C., Inhibitory effect of β-asarone, a component of Acorus calamus essential oil, on inhibition of adipogenesis in 3T3-L1 cells. Food Chem. 2011, 126, 1-7.

Lee, P. Wasting Energy to Treat Obesity. N. Engl. J. Med. 2016, 375, 2298-2300.

Lee, P., Werner, C.D., Kebebew, E., Celi, F.S. Functional thermogenic beige adipogenesis is inducible in human neck fat. Int. J. Obes (Lond). 2014, 38, 170-176.

Lee, Y. H., Mottilo, E. P., Granneman, J. G., Adipose tissue plasticity from WAT to BAT and in between. Biochem. Biophys. Acta 2014, 1842, 358-69.

Lei, F., Zhang, X.N., Wang, W., Xing, D.M., Xie, W.D., Su, H., Du, L.J. Evidence of anti-obesity effects of the pomegranate leaf extract in high-fat diet induced obese mice. Int. J. Obes (Lond). 2007, 31, 1023-1029.

Lim, S., Honek, J., Xue, Y., Seki, T., Cao, Z., Andersson, P. Yang, X., Hosaka, K., Cao, Y. Cold-induced activation of brown adipose tissue and adipose angiogenesis in mice. Nat. Protoc. 2012, 7, 606-615.

Lone, J., Choi, J. H., Kim, S. W., Yun J. W., Curcumin induces brown fat-like phenotype in 3T3-L1 and primary white adipocytes. J. Nutr. Biochem. 2015, 27, 193-202.

Lone, J., Yun, J.W. Honokiol exerts dual effects on browning and apoptosis of adipocytes. Pharmacol. Rep. 2017, 69, 1357-1365.

Lone, J., Yun, J.W. Monoterpene limonene induces brown fat-like phenotype in 3T3-L1 white adipocytes. Life Sci. 2016, 15, 198-206.

Miller, W. C., Swanson, A. B., Phillips, D. H., Fletcher, T. L., Liem, A., Miller, J. A., Structure-Activity Studies of the Carcinogenicities in the Mouse and Rat of Some Naturally Occurring and Synthetic Alkenylbenzene Derivatives Related to Safrole and Estragole. Cancer Res. 1983, 43, 1124-1134.

Mnafgui, K., Derbali, A., Sayadi, S., Gharsallah, N., Elfeki, A., Allouche, N. Anti-obesity and cardioprotective effects of cinnamic acid in high fat diet-induced obese rats. J. Food Sci. Technol. 2015, 52, 4369-4377.

Mosmann, T. Rapid colorimetric assay for cellular growth and survival: application to proliferation and cytotoxicity assays. J. Immunol. Method. 1983, 65, 55-63.

Motillo, E. P., Desjardins, E. M., Crane, J. D., Smith, B. K., Green, A. E., Ducommun, S., Henriksen T. I., Rebalka, I. A., Razi, A., Sakamoto, K., Scheele, C., Kemp, B. E., Hawke, T. J., Ortega, J., Granneman, J. G., Steingberg G. R., Lack of Adipocyte AMPK Exacerbates Insulin Resistance and Hepatic Steatosis through Brown and Beige Adipose Tissue Function. Cell Metab. 2016, 24, 118-129.

Mottillo, E.P., Balasubramanian, P., Lee, Y.H., Weng, C., Kershaw, E.E., Grannemann J.G. Coupling of lipolysis and de novo lipogenesis in brown, beige, and white adipose tissues during chronic β3-adrenergic receptor activation. J. Lipid Res. 2014, 55, 2276-2286.

Ogawa, K., Ito, M., Appetite-Enhancing Effects of Curry Oil. Biol Pharm Bull 2016, 39, 1559-63.

Oi-Kano, Y., Kawada, T., Watanabe, T., Koyama, T., Watanabe, K., Senbongi, R. Iwai, K., Oleuropein, a Phenolic Compound in Extra Virgin Olive Oil, Increases Uncoupling Protein 1 Content in Brown Adipose Tissue and Enhances Noradrenaline and Adrenaline Secretions in Rats. J. Nutr. Sci. Vitaminol. 2008, 54, 363-70.

Parray, H. A., Yun, J. W., Proteomic Identification of Target Proteins of Thiodigalactoside in White Adipose Tissue from Diet-Induced Obese Rats. Int. J. Mol. Sci. 2015, 16, 14441-14463.

Parray, H.A., Yun, J.W. Cannabidiol promotes browning in 3T3L1 adipocytes. Mol. Cell Biochem. 2016, 46, 131-139.

Parray, H.A., Yun, J.W. Combined inhibition of autophagy protein 5 and galectin-1 by thiodigalactoside reduces diet-induced obesity through induction of white fat browning. IUBMB Life 2017, 69, 510-521.

Prabhakar, P.K., Doble, M. Interaction of cinnamic acid derivatives with commercial hypoglycemic drugs on 2-deoxyglucose uptake in 3T3-L1 adipocytes. J. Agric. Food Chem. 2011, 5, 9835-9844.

Qin, B., Panickar, K.S., Anderson, A.R., Cinnamon: Potential Role in the Prevention of Insulin Resistance, Metabolic Syndrome, and Type 2 Diabetes. J. Diabetes. Sci. Technol. 2010, 4, 685 - 693.

Quiroga, P. R., Grosso, N. R., Lante, A., Lomolino, G., Zygadlo, J. A., Nepote, V., Chemical composition, antioxidant activity and anti-lipase activity of Origanum vulgare and Lippia turbinata essential oils. Int. J. Food sci. Tech. 2013, 48, 642-649.

Rafehi, H., Ververis, K., Karagiannis, T.C. Controversies surrounding the clinical potential of cinnamon for the management of diabetes. Diabetes. Obes. Metab. 2012, 14, 493-499.

Rahman, T., Cushing, R. A., Jackson, R. J., Contributions of built environment to childhood obesity. Mt Sinai J Med 2011, 78, 49-57.

Rao, P.V., Gan, S.H. Cinnamon: A Multifaceted Medicinal Plant. Evid. Based. Complement. Alternat. Med. 2014, 642942.

Rashed, A. A., Nawi, M. N. M., Sulaiman, K., Assessment of essential oil as a potential anti-obesity agent: a narrative review. J. Essent. Oil Res. 2017, 29, 1-10.

Ricquier, D. Uncoupling protein 1 of brown adipocytes, the only uncoupler: a historical perspective. Front. Endocrinol (Lausanne). 2011, 2, 85.

Rodriguez, V. M., Portillo, M. P., Pico, C., Macarulla, M. T., Palou, A., Olive Oil Feeding up-Regulates Uncoupling Protein Genes in Rat Brown Adipose Tissue and Skeletal Muscle. Am. J. Clin. Nutr. 2002, 75, 213-20.

Rosen, E.D.; Hsu, C.H.; Wang, X.; Sakai, S.; Freeman, M.W.; Gonzalez, F.J.; Spiegelman, B.M. C/EBPα induces adipogenesis through PPARγ: a unified pathway. Genes. Dev. 2002, 16, 22-26.

Rupasinghe, H. P., Sekhon-Loodu, S., Mantso, T., Panayiotidis, M. I., Phytochemicals in regulating fatty acid β-oxidation: Potential underlying mechanisms and their involvement in obesity and weight loss. Pharmacol. Ther. 2016, 165, 153-63.

Ryu, S., Seol G. H., Park, H., Choi, I. Y., Trans-Anethole Protects Cortical Neuronal Cells against Oxygen-Glucose Deprivation/Reoxygenation. Neurol. Sci. 2014, 35(10), 1541-1547.

Sadiq, S. K., Guixa-Gonzalez, R., Dainesem E., Pastor, M., De Fabritiis, .G, Selent J. Molecular modeling and simulation of membrane lipid-mediated effects on GPCRs. Curr. Med. Chem. 2013, 20, 22-38.

Sangster, S. A., Caldwell, J., Smith, R. L., Metabolism of Anethole. II. Influence of Dose Size on the Route of Metabolism of Trans-Anethole in the Rat and Mouse. Food Chem. Toxicol. 1984, 22, 707-13.

Saponaro, C., Gaggini, M., Carli, F., Gastaldelli, A., The Subtle Balance between Lipolysis and Lipogenesis: A Critical Point in Metabolic Homeostasis. Nutrients 2015, 7,9453-9474.

Seale, P., Conroe, H.M., Estall, J., Kajimura, S., Frontini, A., Ishibashi, J., Cohen, P., Ciniti, S., Spiegelman, B.M. Prdm16 determines the thermogenic program of subcutaneous white adipose tissue in mice. J. Clin. Invest. 2011, 121, 96-105.

Sellayah, D., Sikder, D. Orexin restores aging-related brown adipose tissue dysfun

ction in male mice. Endocrinology 2014, 155, 485-501.

Sharp, L.Z., Shinoda, K., Ohno, H., Scheel, D.W., Tomoda, E., Ruiz, L., Hu, H., Wang, L., Pavlova, Z., Gilsanz, V., et al. Human BAT possesses molecular signatures that resemble beige/brite cells. PLoS One 2012, 7, e49452.

Sheikh, B. A., Pari, L., Rathinam, A., Chandramohan, R., Trans-Anethole, a Terpenoid Ameliorates Hyperglycemia by Regulating Key Enzymes of Carbohydrate Metabolism in Streptozotocin Induced Diabetic Rats. Biochimie 2015, 112, 57-65.

Singh, A. N., Baruah, M. M., Sharma, N., Structure Based docking studies towards exploring potential anti-androgen activity of selected phytochemicals against Prostrate Cancer. Scientific Reports 2017, 7, 1995.

Soliman, M.M.; Attia, H.F.; El-Shazly, A.; Saleh, O.M. Biomedical effects of cinnamon extract on obesity and diabetes relevance in wistar rats. AJMB 2012, 3, 133-145.

Stoner, G. D., Shimkin, M. B., Kniazeff, A. J., Weisburger, J. H., Weisburger, E. K., Gori, GB., Test for Carcinogenicity of Food Additives and Chemotherapeutic Agents by the Pulmonary Tumor Response inStrain a Mice. Cancer Res. 1973, 33, 3069-85.

Subhani, S., Jamil, K., Molecular docking of chemotherapeutic agents to CYP3A4 in non-small cell lung cancer. Biomed. Pharmacother. 2015, 73, 65-74.

Tamura, Y., Iwasaki, Y., Narukawa, M., Watanabe, T. Ingestion of cinnamaldehyde, a TRPA1 agonist, reduces visceral fats in mice fed a high-fat and high-sucrose diet. J. Nutr. Sci. Vitaminol (Tokyo). 2012, 58, 9-13.

Tan, C.Y., Ishikawa, K., Virtue, S., Vidal-Puig, A. Brown adipose tissue in the treatment of obesity and diabetes: Are we hot enough?. J. Diabetes Investig. 2011, 2, 341-350.

Tiraby, C., Tavernier, G., Lefort, C., Larrouy, D., Bouillaud, F., Ricquier, D., Langin, D. Acquirement of brown fat cell features by human white adipocytes. J. Biol. Chem. 2003, 278, 33370-33376.

Truhaut, R., Le Bourhis, B., Attia, M., Glomot, R., Newman, J., Caldwell, J., Chronic Toxicity/Carcinogenicity Study of Trans-Anethole in Rats. Food Chem. Toxicol. 1989, 27, 11-20.

Tung, Y. C., Hsieh, P. H., Pan, M. H., Ho, C. T., Cellular models for the evaluatio n of the antiobesity effect of selected phytochemicals from foods and herbs. J Food Drug. Anal. 2017, 25, 100-110.

van Marken Lichtenbelt, W. D., Vanhommerig, J. W., Smulders, N. M., Drossaerts, J. M., Kemerink, G. J., Bouvy, N. D., Scharuwen, P., Teule, G. J., Cold-acti vated brown adipose tissue in healthy men. N. Engl. J. Med. 2009, 360, 1500 -8.

Vermaak, I., Hamman, J. H., Vilijoen, A. M., Hoodia gordonii: an up-to-date revie w of a commercially important anti-obesity plant. Planta. Med. 2011, 77, 114 9-60.

Verspohl, E.J., Bauer, K., Neddermann, E. Antidiabetic effect of Cinnamomum cassi a and Cinnamomum zeylanicum in vivo and in vitro. Phytother. Res. 2005, 1, 203-206.

Virtanen, K. A., Lidell, M. E., Orava, J., Heglind, M., Westerngren, R., Niemi, T. T aittonen, M., Laine, J., Savisto, N. J., Enerback, S., Nuutilla, P., Functional b rown adipose tissue in healthy adults. N. Engl. J. Med. 2009, 360, 1518-25.

Wang, C., Xia, T., Du, Y., Meng, Q., Li, H., Liu, B., Chen, S., Guo, F., Effects of ATF4 on PGC1α expression in brown adipose tissue and metabolic response to cold stress. Metabolism 2013, 62, 282-289.

Wang, T.Y.; Liu, C.; Wang, A.; Sun, Q. Intermittent cold exposure improves gluco se homeostasis associated with brown and white adipose tissues in mice. Li fe Sci. 2015, 15, 153-159.

Weikel, K. A., Ruderman, N. B., Cacicedo, J. M., Unraveling the actions of AMP-a ctivated protein kinase in metabolic diseases: Systematic to molecular insigh ts. Metabolism 2016, 65, 634-645.

Wizzler, L. A. M., Silva-Comar, F. M., Silva-Filho, S. E., Oliveria, M. J. A., Bersa ni-Amando, C. A., Cuman, R. K. N., Evaluation of immunomodulatory activi ty of trans-anethole and estragole, and protective effect against cyclophccco sphamide-induced suppression of immunity in Swiss albino mice. Int. J. Ap pl. Res. Nat. Prod. 2015, 8, 26-33.

Yamaguchi, M., Baile, C.A., Zhu, S., Shoji, M. Bioactive flavonoid p-hydroxycinna mic acid stimulates osteoblastogenesis and suppresses adipogenesis in bone

marrow culture. Cell Tissue Res. 2013, 354, 743-750.

Yin, W., Mu, J., Birnbaum, M.J. Role of AMP-activated protein kinase in cyclic AMP-dependent lipolysis in 3T3-L1 adipocytes. J. Biol. Chem. 2003, 278, 43074-43080.

Zhang, W., Li, X., Yu, T., Yuan, L., Rao, G., Li, D., Mu, C., Preparation, physiochemical characterization and release behavior of the inclusion complex of trans-anethole and β-cyclodextrin. Food Resear. Internati. 2015, 74, 55-62.

Zhao, H., Xie, Y., Yang, Q., Cao, Y., Tu, H., Cao, W., Wang, S. Pharmacokinetic study of cinnamaldehyde in rats by GC-MS after oral and intravenous administration. J. Pharm. Biomed. Anal. 2014, 89, 150-157.

# 갈색지방화에 의한 *trans*-anethole 및 *trans*-cinnamic acid의 항 비만효과

강 남 현

대구대학교 대학원
석사과정 생명공학과

지도교수 윤 종 원

(초록)

최근 백색 지방세포의 갈색지방화 (browning)와 갈색 지방세포의 활성화를 이용하는 방법이 비만 예방을 위한 좋은 전략이 되고 있다. 특히 갈색 지방화 활성이 있는 천연 화합물들을 이용한 항비만 치료제 개발이 활기를 띠고 있다. 본 연구에서는 다양한 식물의 필수 지방에 존재하는 향미 물질인 *trans*-anethole (TA)과 계피껍질에 존재하는 *trans*-cinnamic acid (*t*CA)이 백색 지방세포를 갈색 지방화 세포로 유도한다는 사실을 입증하였다. TA와 *t*CA는 백색 지방세포에서 갈색 지방 마커 단백질 (PGC-1α, PRDM16, UCP1)의 함량과 갈색지방화된 지방세포 (베이지 지방)의 특이 유전자 (*Cd137, Cited1, Tbx1, Tmen26*)의 발현 수준을 증가시키고, HIB1B 갈색 지방세포에서 갈색 지방 특이 적 유전자 (*Cidea, Lhx8, Ppargc1, Prdm16, Ucp1* 및 *Zic1*)의 발현을 증가시켰다. 또한 TA와 *t*CA는 3T3-L1 백색 지방 세포의 지방 산화를 증가시키고 지방 생성을 감소시켰으며, HIB1B 갈색 지방 세포를 활성화시켰다. 또한 지방대사에서는 TA와 *t*CA가 β3-AR 및 AMPK 신호 전달 경로의 활성화를 통해 3T3-L1 백색 지방 세포의 갈색 지방화를 유도한다는 사실을 알아냈다. 특히, TA는 β3-AR뿐만 아니라 AMPK 매개체인 SIRT1 경로의 조절을 통해서도 갈색 지방화를 유도하였다. 결론적으로, TA와 *t*CA는 백색지방세포의 갈색화 전환과 동시에 갈색지방을 활성화시키는 기능에 의하여 에너지 대사를 크게 증가시킴으로써 비만 치료제로서의 가능성을 보여주었다.